Spring 2023

Development of Interatomic Potential of High Entropy Diborides With Artificial Intelligence Approach to Simulate the Thermo-Mechanical Properties

Nur Aziz Octoviawan
Missouri State University, Octoviawan7@MissouriState.edu

Follow this and additional works at: https://bearworks.missouristate.edu/theses

Part of the Atomic, Molecular and Optical Physics Commons, Ceramic Materials Commons, Engineering Physics Commons, and the Other Materials Science and Engineering Commons

Recommended Citation

Octoviawan, Nur Aziz, "Development of Interatomic Potential of High Entropy Diborides With Artificial Intelligence Approach to Simulate the Thermo-Mechanical Properties" (2023). *MSU Graduate Theses.* 3835.
https://bearworks.missouristate.edu/theses/3835

DEVELOPMENT OF INTERATOMIC POTENTIAL OF HIGH ENTROPY DIBORIDES WITH ARTIFICIAL INTELLIGENCE APPROACH TO SIMULATE THE THERMO-MECHANICAL PROPERTIES

A Master's Thesis

Presented to

The Graduate College of

Missouri State University

In Partial Fulfillment

Of the Requirements for the Degree

Master of Science, Materials Science

By

Nur Aziz Octoviawan

May 2023

DEVELOPMENT OF INTERATOMIC POTENTIAL OF HIGH ENTROPY DIBORIDES WITH ARTIFICIAL INTELLIGENCE APPROACH TO SIMULATE THE THERMO-MECHANICAL PROPERTIES

Physics, Astronomy, and Materials Science

Missouri State University, May 2023

Master of Science

Nur Aziz Octoviawan

ABSTRACT

The interatomic potentials designed for binary/high entropy diborides and ultra-high temperature composites (UHTC) have been developed through the implementation of deep neural network (DNN) algorithms. These algorithms employed two different approaches and corresponding codes; 1) strictly local & invariant scalar-based descriptors as implemented in the DEEPMD code and 2) equivariant tensor-based descriptors as included in the ALLEGRO code. The samples for training and validation sets of the forces, energy, and virial data were obtained from the ab-initio molecular dynamics (AIMD) simulations and Density Functional Theory (DFT) calculations, including the simulation data from the ultra-high temperature region (> 2000K). The study then compared the accuracy of the Deep Learning potentials to predict not only the ground-state properties, such as the elastic constants and the phonon dispersion curves but also the ultra-high temperature properties, including the lattice parameters and melting behaviors.

DEVELOPMENT OF INTERATOMIC POTENTIAL

OF HIGH ENTROPY DIBORIDES WITH ARTIFICIAL INTELLIGENCE APPROACH

TO SIMULATE THE THERMO-MECHANICAL PROPERTIES

By

Nur Aziz Octoviawan

A Master's Thesis
Submitted to the Graduate College
Of Missouri State University
In Partial Fulfillment of the Requirements
For the Degree of Master of Science, Materials Science

May 2023

Approved:

Ridwan Sakidja, Ph.D., Thesis Committee Chair

Kartik Ghosh, Ph.D., Committee Member

Tiglet Besara, Ph.D., Committee Member

Julie Masterson, Ph.D., Dean of the Graduate College

ACKNOWLEDGEMENTS

I dedicate this thesis to my wife, Ghiska Ramahdita & my son Austenio Zahid Sonazka.

TABLE OF CONTENTS

LIST OF TABLES

LIST OF FIGURES

INTRODUCTION

In recent years, materials development has been heavily loaded with simulation processes. An innovative approach to speed up the discovery of materials. This method is also an effective and efficient way to understand the behavior of materials in extreme environments. For example, materials that can withstand high-temperature applications will benefit from the modeling approach since testing the material with the actual application would require a lot of resources. Candidates for this application are transition metal diborides, for example, zirconium diboride, hafnium diboride, and titanium diboride. Each of the materials has promising properties. Currently, those ultra-high temperature composites (UHTC) are widely used in spacecraft or reentry vehicles that need to maintain stability at extreme Temperatures. This material's distinct properties, such as high thermal conductivity, high resistance to thermal shock, and high melting temperature above 3000 K [1-2], give this material a great candidate to develop material that can withstand elevated temperatures.

Due to their oxidation and thermal shock resistance, the properties are also fundamental to making ultra-high-temperature ceramics. Each binary has its advantage; for instance, zirconium diboride, this material being identified as the material with the lowest density among other diborides [1-4]. The other diboride pair, such as hafnium diboride also being investigated to be one other ultra-high temperature ceramic.

Understanding that each component will have its strength, nowadays, scientists have taken a new step in the development of UHTC by adding a dopant to increase its properties. However, with an excellent alloying process recently, scientists are now taking an even further step, combining up to five elements of diboride and creating a high entropy material. The

breakthrough technology in alloying process increases the materials' properties, hoping that the material will absorb the strength of each binary diboride.

High Entropy Diboride

Traditionally, the materials are developed by one or two bulk components with the additive (dopant) for the other elements to enhance their properties, such as the corrosion properties, the mechanical, melting point, electrical or magnetic properties. Several studies still heavily researched this to find the best properties the materials can achieve. In recent years, the trend has been to expand compositional space into more complex material. This development is called high entropy materials, which are vastly growing in the metallurgy aspect.

High Entropy Alloys (HEAs) are also known as complex, concentrated alloys, or multiracial alloys, commonly consisting of a minimum of 5 elements with a composition between 5 -35% of each component. [5 – 6]. The configurational entropy can reach a significant amount once five or more principal members are present in the system; it comes to a maximum value of $\Delta S_{mix} = R \ln N$ per mole for an N-component system, where R is the gas constant for an equimolar composition.

Miracle and Senkov (2017) gave an extensive review of the main principles and predominant properties of high entropy materials [5], with the emphasis being given to four distinct aspects:

"The high entropy effect" – increases the configurational entropy of five elements or more. The effect can help stabilize the solid solution over intermetallic or other complex phases. This argument has been used to suggest increased stability at higher temperatures as entropy linearly increases with temperature.

The second aspect is lattice distortion, in which a significant mismatch between the atomic size of the principal component would increase the distortion more than the conventional alloys.

The subsequent effect is called the sluggish diffusion effect, which means the diffusion process on the high entropy alloys will be slow due to the formation of nanocrystals and amorphous phases upon cooling.

The last effect is called the cocktail effect, a qualitative statement that the material produced will be more beneficial than a member of their constituent since they will benefit from their constituent and have distinct properties quite different from their component.

The first high entropy alloys were introduced by Cantor (2004) with the production of Fe20Cr20Mn20Ni20Co20-based alloys that are stabilized into a single FCC phase.[7]

Structure of Transition Metal - Diboride

Transition metal diborides, such as hafnium diboride, tantalum diboride, titanium diboride, zirconium diboride, niobium diboride, and molybdenum diboride, have a crystal structure that categorized as hexagonal structure, with the space group p6/mmm. The crystal structure has two layers, one is Boron, and the other is transition metal. Both layers are alternating. From the top view, a 6-atom ring of Boron will surround the transition metal atom. The boron-boron atom bond is covalent, while each transition metal bond has a metallic bond.

Transition metal diborides are a class of ceramic materials that have a unique crystal structure. They consist of two boron atoms and a transition metal atom that form a hexagonal lattice. Each transition metal atom is surrounded by two boron atoms above and below the plane

of the lattice. The crystal structure of transition metal diborides can be described as a layered

structure with a space group of P6/mmm, as shown in Figure 1.
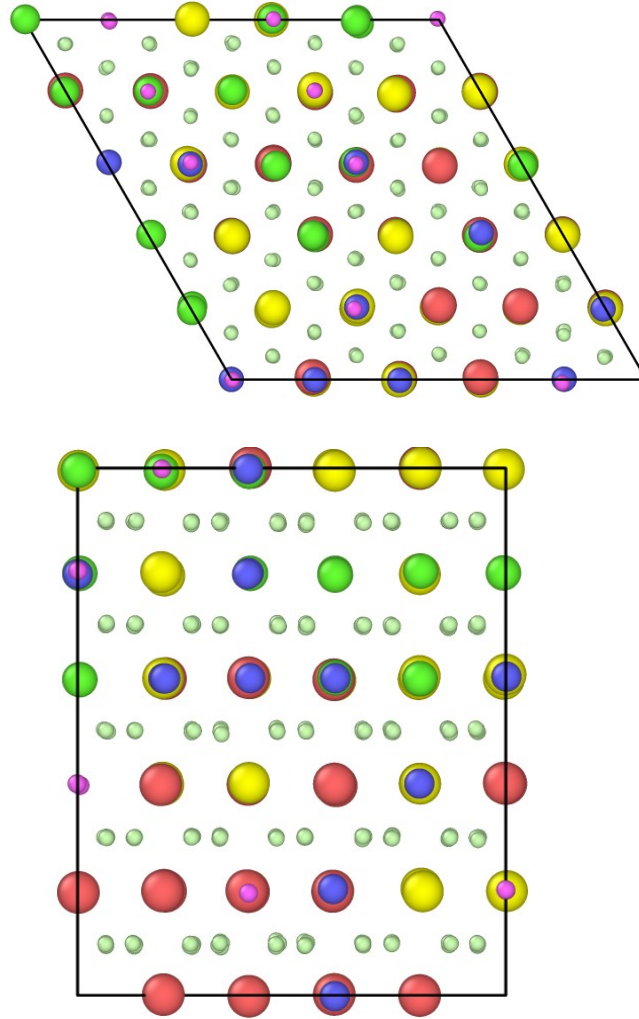
Figure 1. Schematic Structure of High Entropy Diborides, with five elements Transition Metals. The Hexagonal p6/mmm symmetry

The lattice parameters of transition metal diborides vary depending on the specific

transition metal used. The experimental lattice parameter studied in this research can be seen in

Table 1 as follows.

Table 1. Lattice Parameter of Studied HEA Diboride, HfZrTaNbTiB2, and HfZrTaMoTiB2 [8]

Composition	Single Phase	a(Å)		c(Å)		Relative Density
		Average	XRD	Average	XRD	
$(Hf_{0.2}Zr_{0.2}Ta_{0.2}Nb_{0.2}Ti_{0.2})B_2$	Yes	3.11	3.101	3.346	3.361	92.40%
$(Hf_{0.2}Zr_{0.2}Ta_{0.2}Mo_{0.2}Ti_{0.2})B_2$	Yes	3.093	3.08	3.307	3.316	92.40%

The electronic structure of transition metal diborides is characterized by the partially filled d-orbitals of the transition metal atoms, which give rise to metallic conductivity. The coordination number of the transition metal atoms is typically 6, forming an octahedral coordination geometry. The crystal structure makes them attractive for various applications, including high-temperature superconductors, hard coatings, and catalysts.

Within the boron planes, the boron atoms form a network of triangles, with the metal atoms occupying the interstitial sites. The boron atoms are covalently bonded to each other and the metal atoms, while the metal atoms are bonded via metallic bonding. The bonding between the metal and boron atoms is a combination of covalent and ionic bonding, with the exact nature of the bonding depending on the specific transition metal and the crystallographic direction. The coordination number of the metal atoms is typically 12, with six boron atoms and six metal atoms in the first coordination shell.

Overall, the crystal structure of transition metal diborides is highly ordered and simple, despite the high degree of anisotropy in its properties. This simplicity, combined with its excellent mechanical, thermal, and electrical properties, has led to extensive research into its potential applications in various fields, including aerospace, energy, and electronics.

Density Functional Theory

Density Functional Theory (DFT) is a method based on computational aiming to study the electronic structure of the materials [9]. It is based on the concept that the total energy of a system can be expressed as a function of electron density rather than the wave function of the electrons, which is computationally expensive to calculate.

On DFT calculations, the electronic structure is defined as a function of the electron's position. Then, the system's total energy is based on calculating the electron density by solving the Kohn-Sham equation. The energy total has components from kinetic energy, the electrostatic interaction from each electron, and exchange-correlation energy. In 1964, Hohenberg and Kohn finally formulated the density functional theory that turned complicated many-electron wavefunctions containing 3N (N being the number of electrons for three spatial variables) into three spatial variables [10]. The reduction of these many-body problems came only a year later by Kohn and Sham by simplifying multi-electron problem into an issue of non-interacting electrons in an effective potential which includes interaction between electrons, the exchange, and correlation interactions [11]

$$H = T_N + T_e + V_{N-N} + V_{e-e} + V_{N-e} \qquad (1)$$

Herein, T_N represents the kinetic energy for the nuclei, T_e the kinetic energy for electrons, V_{N-N} the potential energy for nucleus-nucleus interaction, V_{e-e} the potential energy for electron-electron interaction, V_{N-e} It is defined as the potential energy for nucleus-electron interaction.

Molecular Dynamics Simulation

Molecular dynamics is a method to simulate solids. The technique can handle particle numbers in many orders of magnitude compared to the ab initio approaches. In Figure 2, the comparison of each approach on different time scales and sizes of the model can be seen. Physical science can predict system behavior with the caveat that there is a detail that sufficient. For example, classical mechanics provides a method that predicts future actions if all related mechanisms are understood well. The object's mass, position, and velocity, Laplace, determines the whole trajectory by referring to the Newtonian equation of motion.
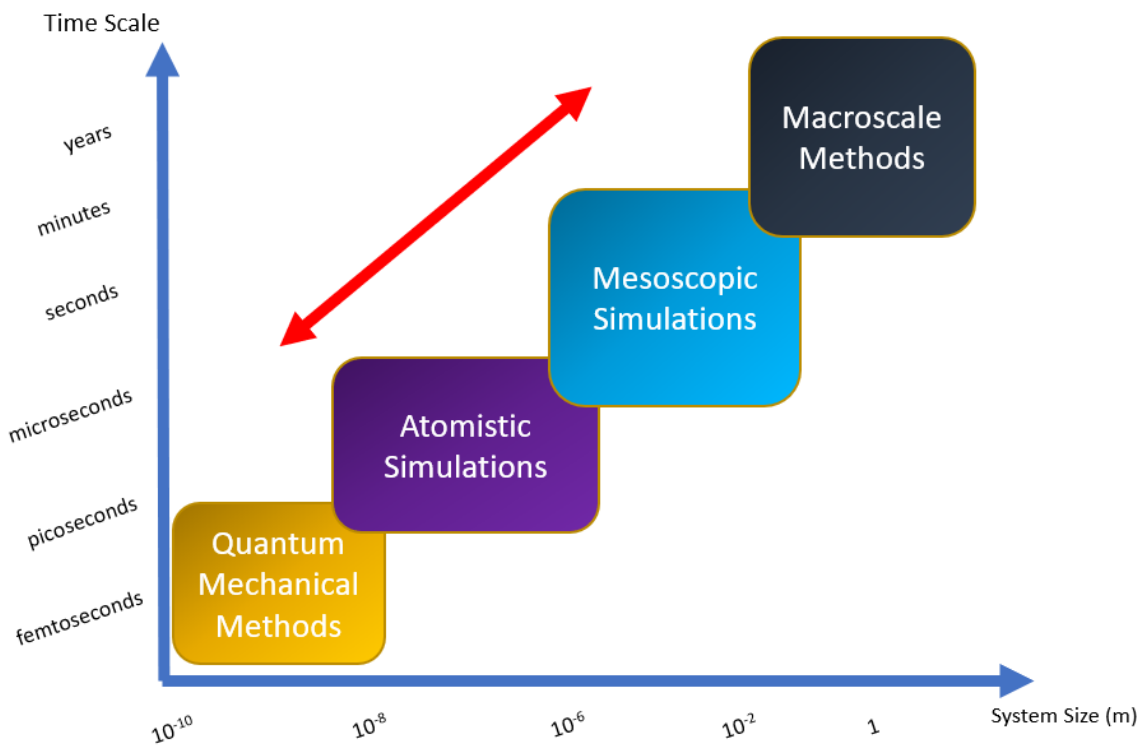
Figure 2. Schematic diagram showing different simulations in time and length scale

The machine learning interatomic potential and the utility of this molecular dynamics simulation are connected with generating an accurate potential energy surface (PES) representation. This landscape underpins reactivity, phase stability, and other observable properties. As discussed, the PES is typically obtained using Quantum mechanic calculation with Density functional theory. Still, there is a reasonably high cost associated with the level of theory used to approximate solutions to the Schrödinger equation. The "holy grail" for developing interatomic potential with machine learning based on computational scientists can create the interatomic potential with a reasonably simple dataset with exceptionally accurate PESs.

With a system that has more than 100 atoms, the computational requirement of Quantum Mechanics (QM) methods is significantly increased. As compensation, the computational scientist will degrade the dimension with lower-dimensional representations, reducing the PES details for efficiency. Also, this limits our ability to comprehend higher-order systems, particularly as they pertain to their fundamental properties, which inevitably demand a large-scale model to simulate.

Fortunately, this accuracy–efficiency trade-off, classically thought of as pervasive and unavoidable, is beginning to be overcome by the rapid expansion of machine-learned interatomic potentials (MLIP). As shown in Figure 3, it can be seen the comparison between the emerging method of MLIP enables us to extend our modeling capability to a more significant number of atoms due to its inherent linear scaling.
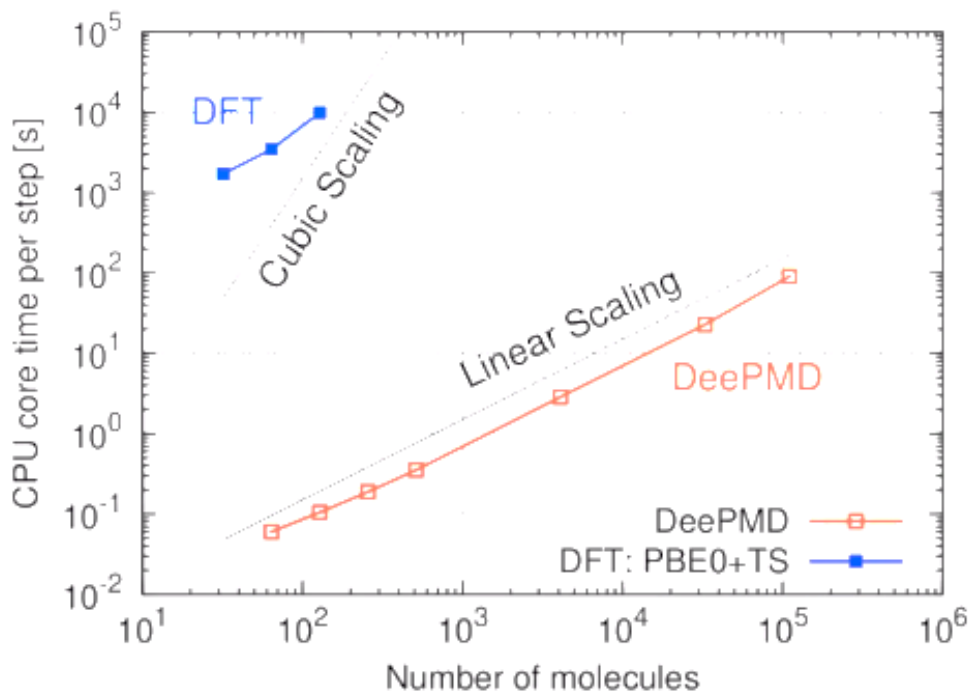
Figure 3. Comparison of DFT calculation vs. DeePMD, Machine learning based Interatomic Potentials, towards the number of molecules can be simulated and CPU resources required

Neural Network Interatomic Potential of Molecular Dynamics

Machine-learning interatomic potentials (MLIP) have become a potent tool to simulate the behavior and properties of materials. Interatomic potentials are developed to predict the potential energy (together with its derivatives), which comes from the interaction of a variable-size atomic system as a function of atomic positions and types. The MLIP offers a different approach compared to the previous empirical potential, which can improve the result of Prediction. The model hopes to model various chemical compositions, bonding types, or levels of the approximated quantum-mechanical theory. Currently, the research goal will focus on developing the potential to achieve better accuracy, efficiency, and transferability.

MLIP was started by Behler and Parrinello (2006). This approach can approximate the potential energy on the surface, which then looks like a promising technique for using neural

networks as a functional form of interatomic potentials, going beyond the small molecular systems by employing the locality of interaction [12-13].

The structure of potentials commonly contains two parts: descriptors and three bodies. The descriptors are usually used for describing the local atomic environments that will capture the physical interaction, and then the regressor, which is a function that maps the descriptors to the energy interaction. MLIP primarily uses the neural network as the first and most widely used regressor [13–19]. The other popular interatomic potential class is message-passing potentials, based on neural networks. But then capture also beyond the local descriptors of atomic environments [20-22]. MLIPs can be constructed using numerous techniques, such as neural networks, reinforcement learning, or kernel methods.

The fact that empirical MLIPs are approximate models of fundamental physics and chemistry and must thus be adapted to replicate reference data from experiments or quantum calculations is a crucial restriction of these models. Recent advances in ML approaches have made it possible to create MLIP with accuracy that rivals that of quantum computations with evaluation times that scale linearly. This results in significant computational savings over quantum mechanics because they naturally can acquire detailed, non-linear functional mappings that connect the inputs to the intended outcomes. Yet, machine learning interatomic potentials (MLIPs) still struggle to achieve a wide range of transferability. Even though, currently, some significant advancements in the complexity of the behavior may be captured with ML-based models. Figure 4 shows five aspects of defining an excellent interatomic potential. Known as the Holy Grail of MLIP, it covers efficiency, transferability, and accuracy.
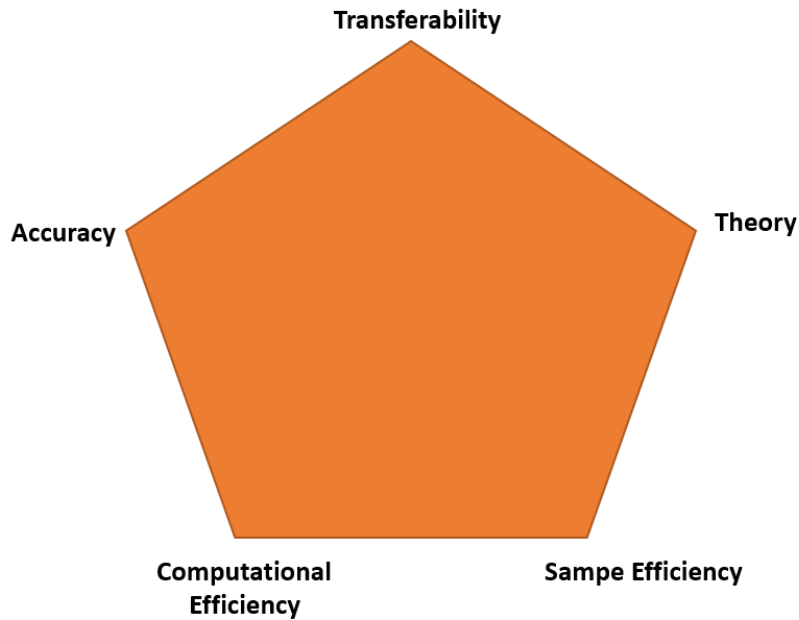
Figure 4. Five Aspects of Effective Machine Learning Interatomic Potential

DeePMD Simulation Package

DeePMD is a code that can be used to develop machine learning interatomic potential [22]. The code interfaces with TensorFlow, which allows training, testing, and evaluation of the potential energy surface and the forces and interfaces with molecular dynamics simulation, such as LAMMPS [23].

The basic concept of the DeePMD-kit is implementing the atomic environment descriptors and chain rules for force/viral computations in C++ and providing an interface to incorporate them as new operators in standard TensorFlow. The theory of DeePMD is to consider a system with N atoms, and then each atom will denote by each coordinate. $(R_1 \ldots R_N)$. Then the potential energy of the system $€$ is a function of 3N variables $E = E(R_1 \ldots R_N)$. In the DeePMD method, the total energy is the sum of each representation of energy per atom.

$$E = \sum_i Ei \qquad (2)$$

With i being the index of the atom. The i-th atom's position and the neighbor's energy determine the atom's position.

$$Ei = Es(i)(Ri, \{Rj \mid j \in NRc\,(i)\}) \qquad (3)$$

The most straightforward idea to model the atomic energy Es(i) through DNN is to train a neural network with the input simply being the positions of the i-th atom Ri and its neighbors $\{Rj \mid j \in NRc(i)\}$. NRc (i) will represent the index set of the neighbors of atom i within the cutoff radius Rc, i.e., Rij = |Rij | = |Ri – Rj | ≤ Rc. s(i) is the chemical species of atom i.

Figure 5 simplifies the schematic of how the coordinate materials will translate to energy. As discussed, the total energy is calculated from each energy per atom, translated from each atom's environment.
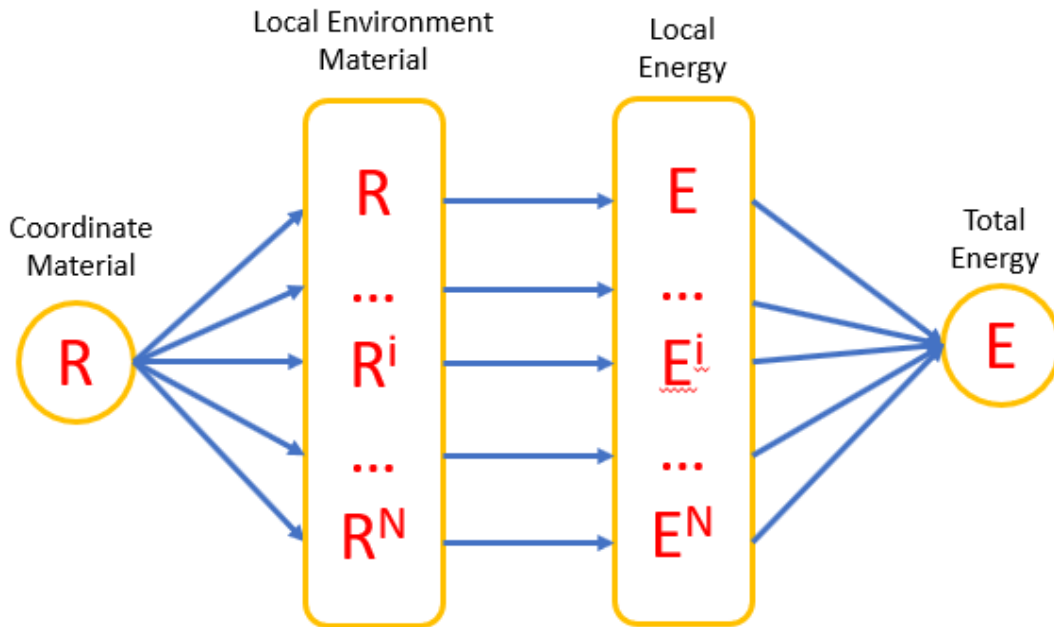
Figure 5. Schematic for neural networks inside the DeePMD and the flow to represent local energy

12

The workflow of the DeePMD is defined into four three steps of the process. The data

generator comes from the calculation of DFT, Ab-initio Molecular Dynamics (AIMD), or

Quantum Monte Carlo (QMC). This study uses DFT calculation with the Vienna ab-initio

Simulation Package (VASP) software as our data generator. Then the process continues to the

DeePMD train or test, which processes all the data into the architecture on the DeePMD kit. It

consists of raw data translated to descriptors before coming to the DeePMD network and will

give the result about the Prediction of energy, forces, and virial. And the next step is the interface

of the DeePMD model to molecular dynamics simulation. In this study, I use LAMMPS as the

molecular dynamics simulation to simulate the potential to be the desired materials as the target

of this study. The schematic plot of this DeePMD process can be found in Figure 6.
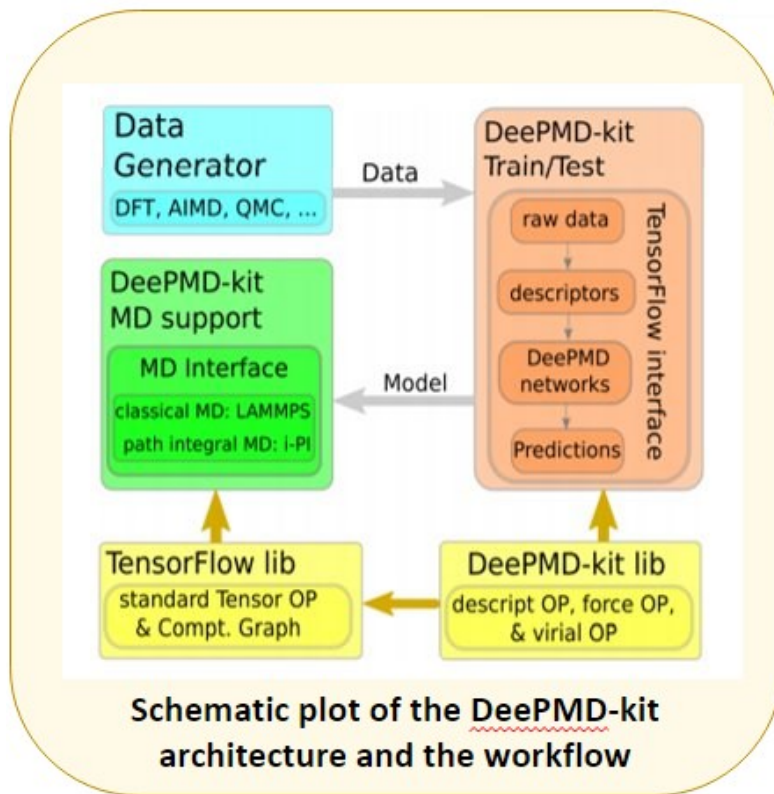
Figure 6. DeePMD architecture and workflow

The first process is data preparation. The data from the DFT calculation will comprise a list of systems containing many frames. The frames are used as the training data. And the rest will be used for testing. The records show the tensor shape found on each frame and the atom's position in that system. The DeePMD kit defines data protocol which is called RAW format. This file will serve as training/test data. The box tensor, coordinate atom, and label (to define the materials) will be stored in a separate text file box. raw, coord.raw, force.raw, virial.raw, and type.raw (atom types). The whole file, except for type. raw will convert to binary files and set as the training/test data for DeePMD.

Allegro Simulation Package

Allegro is equivariant deep learning with an approach to retain the high accuracy of the recently proposed class of equivariant message passing neural network (MPNN) while combining to strict locality so it will have the ability to have accuracy in an extensive system [24].

Message-passing neural networks (MPNN) based on learned atomistic representations operate on an atomistic graph constructed by representing atoms as nodes and defining edges between atoms within a fixed cutoff distance of one another. In Allegro, the code is developed with a strict locality, as the conventional MPNN has some scalability and memory consumption issues.

The equivariant neural networks are coming to preserve them from the physics of atomic systems under the action of several geometric symmetries—rotation, inversion, and translation—which together comprise the Euclidean group E (3) (rotation alone is SO (3), and rotation and inversion together include O (3)). Scalar quantities, such as the potential energy, are invariant to these symmetry group operations. In contrast, vector quantities such as the atomic forces are

equivariant to them and transform correspondingly when the atomic geometry is changed [24-25].

Each atom's hidden, latent space is a feature vector consisting solely of invariant scalars for the invariant, atom-centered message-passing interatomic potentials. The existing machine Learning interatomic potential, such as DeePMD, guarantees the invariance of their predicted energies by acting only on invariant inputs. On the equivariant neural networks, the developed network can work directly on non-invariant geometric inputs, like displacement vectors, in a symmetry-respecting way, achieved by using only E (3)-equivariant operations, yielding a model whose internal features are equivariant to the 3D Euclidean group.

Unlike DeePMD, which uses the invariant and the energy decomposition represented per atom energy, Allegro's decomposition process uses pairwise energy decomposition. Blue represents the scalar, while red represents the tensor function of energy decomposition. As seen in Figure 7, the decomposition process of the energy is defined as hij, which comes from the interaction of atom i and atom j.
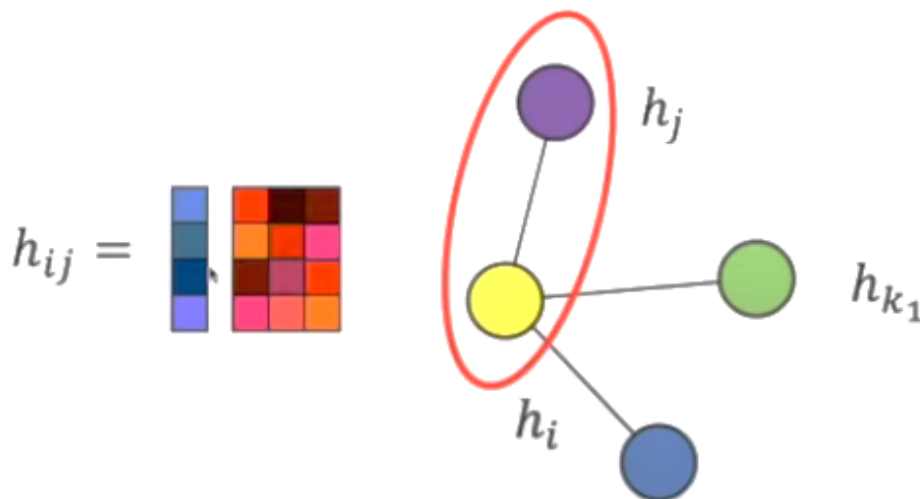
Figure 7. Method of Decomposition for Energy from Allegro, with Pairwise energy

The Allegro approach begins by breaking down a system's potential energy into per-atom energies Ei per the earlier methods.

$$Esystem = \sum_{i}^{N} \sigma_{Zi} Ei + \mu_{Zi} \qquad (4)$$

The σ_{Zi} and μ_{Zi} are potentially trainable per-species scale and shift settings. Then it further divides the per-atom energy into a sum of pairwise energies, indexed by the core atom and one of its neighbors, in contrast to most existing MLIPs.

$$E_i = \sum_{j \in \aleph(i)} \sigma_{Zi,Zj} Eij \qquad (5)$$

Now, j covers the neighbors of atom i, and once again, a per-species-pair scaling factor of Zi,Zj is optional. The atom i and its neighbor j serve as the index for these pairwise energies, but other nearby atoms k in the local environment N(i) may also play a role. In Allegro, Eij and Eji only depend on the surroundings of the corresponding central atoms because they each contribute differently to the site energies Ei and Ej, respectively. Eij and Eji as a result and on purpose.

The Allegro architecture, depicted in Figure 8, is a Nlayer ≥ 1 layer, arbitrarily deep, equivariant neural network. Using two latent spaces—an equivariant latent space, which processes tensors of any rank l ≥ 0, and an invariant latent space, which processes scalar (l = 0) features—the architecture learns representations linked to ordered pairs of surrounding atoms. At every layer, the two latent spaces communicate with one another. A multi-layer perceptron (MLP) acting on the scalar characteristics of the last layer is then used to compute the final pair energy Eij.
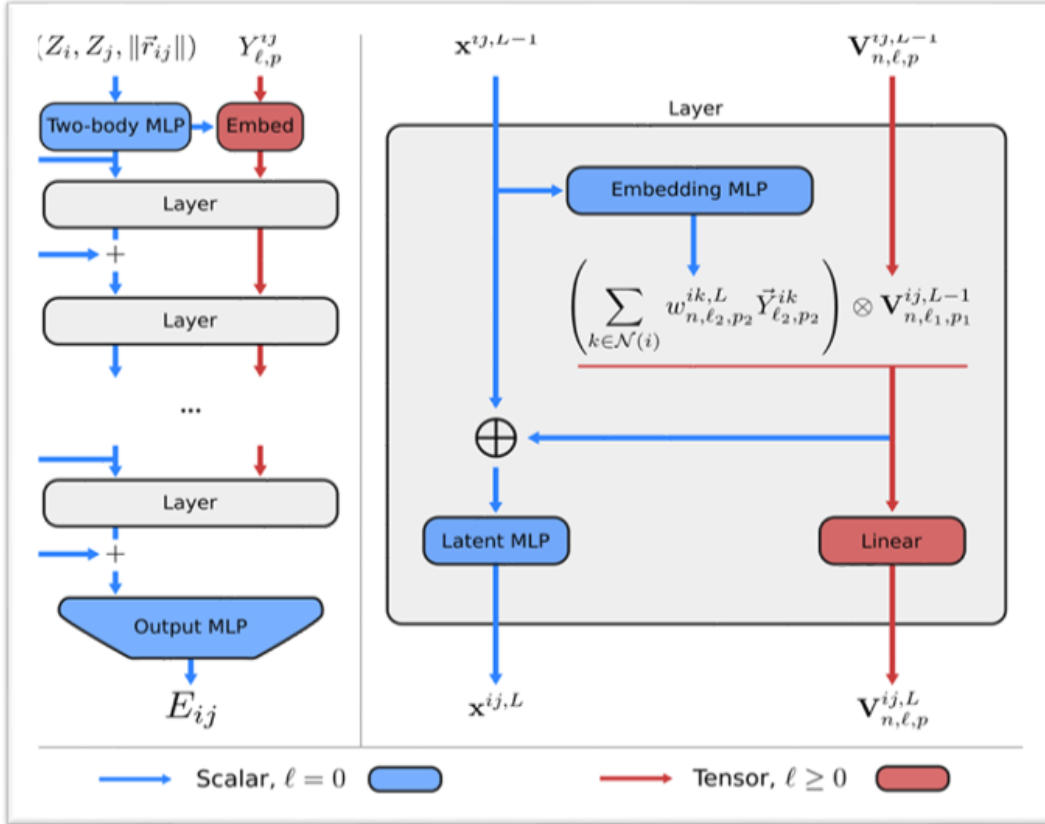
Figure 8. Allegro model architecture and details of a tensor product layer. Blue represents the scalar, and red represents the tensor.

Active Learning

The new development of neural network development is called active learning. The Active learning technique is coming because the most time-consuming part of the development is defining and establishing the best training set based on trial-and-error iterations. The training set can be verified while all the steps are already followed and potential already developed, which will need a complete cycle of the method. The dataset needs to be manually assessed for the performance of the trained potential and tries to understand how to construct configurations for the new training set to avoid the undesirable behavior of the potential on the next iteration. The method called Active Learning is a technique that is based on machine learning that will do the learning in the

middle of the process of MLIP development. This technique allows the refinement iterations to a computer, which will automate updating the dataset based on the learning process[26].

The concept of active learning, which can be retroactively characterized as a learning-and-forgetting scheme, originates from the idea of active learning during atomistic simulations. The first learning-and-remembering technique was put forth in, but the sampling was uniform; a predetermined amount of time steps was skipped before including a configuration in the training set, which would otherwise continue to grow indefinitely. Under this plan, the training set would comprise some of the final arrangements along the track of molecular dynamics.

COMPUTATIONAL METHODS

Density Functional Theory Calculation (Vienna Ab-initio Simulation Package)

The primary data generated in this research was based on density functional theory and ab-initio calculation. Before the calculation process, some input must be ready to run the analysis. The first input for this calculation is POSCAR, which is the crystal structure of the materials that need to be calculated. In this research, the volume of the POSCAR was varied into five different scales for each composition. In this research, the standardized structure of the POSCAR that I used for the training and validation sets contains 24 atoms, eight transition metals, and 16 Boron atoms. A schematic visualization generated by OVITO[27] to represent a typical POSCAR structure can be found in Figure 9.
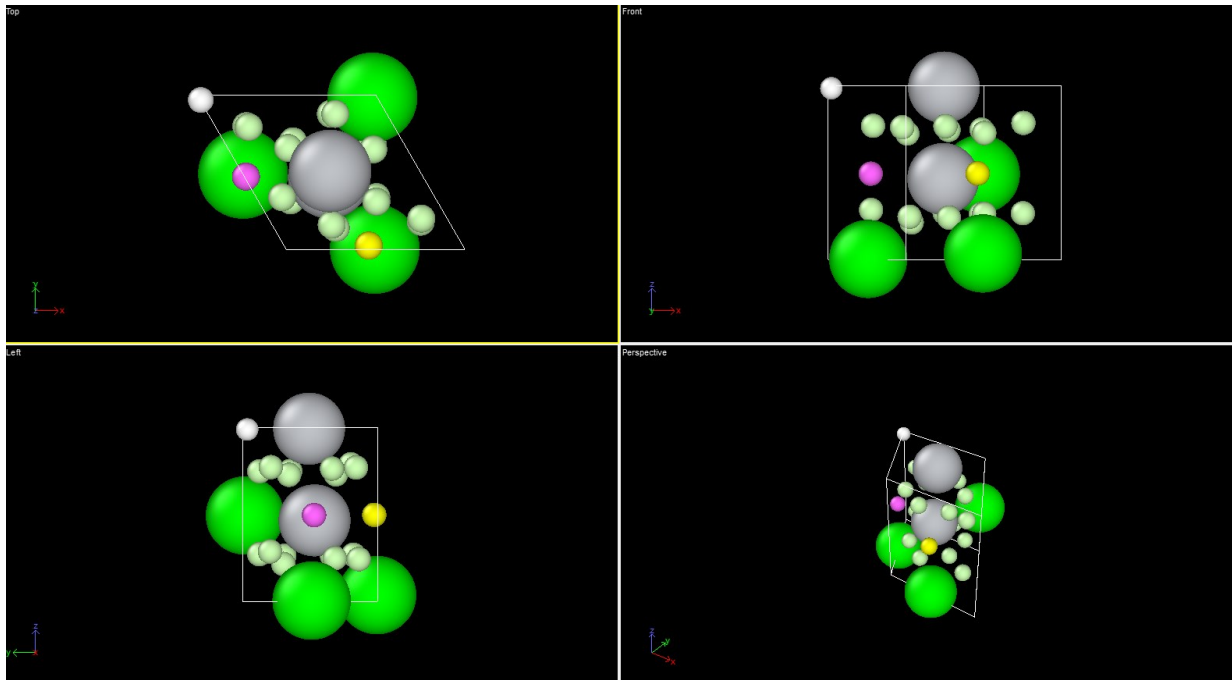
Figure 9. Visualization of POSCAR file of input from DFT Calculation

The other additional input files necessary for the DFT calculations are the INCAR and

KPOINTS files. For all calculations, the standardized KPOINTS was set to 3x3x3,

corresponding to the k-point grid used. The INCAR file is the main input file for the VASP code.

For the ab-initio MD simulations, the files are also used to specify the simulation temperature.

The PREC is set as Accurate with cutoff energy (ENCUT) set at 450eV. The details of the

INCAR file can be seen in Figure 10. Further explanation regarding the rest of the input

parameters defined within the INCAR file can be found at

https://www.vasp.at/wiki/index.php/Input.


```
SYSTEM=HEA_MB2
PREC=Accurate
ENCUT=450 # ENMAX in POTCAR
NELM=200
#NBANDS=84
#KPAR=8
NELMIN=10
EDIFF=1.0e-8
EDIFFG=1E-6
NSW=500
NBLOCK=1
KBLOCK=1000
IBRION=0
POTIM=1.00 # time fs
ISIF=2
ISMEAR=0
SIGMA=0.05
LPLANE=.TRUE.
LREAL=.TRUE.
VOSKOWN=0
ALGO=Normal
LWAVE=.FALSE.
LCHARG=.FALSE.
MAXMIX=30
ISYM=0
SMASS=0
TEBEG=3500
TEEND=3500
```

Figure 10. Standardized INCAR file of DFT calculation with the variable of temperature in 3500K and ALGO Normal

The composition prepared for the calculation is based on six elements of transition metal diborides: Hf, Ta, Zr, Mo, Ti, B (HEA_MB2_Mo) and Hf, Ta, Zr, Nb, Ti, B (HEA_MB2_Nb). The calculation of each diboride compound started with a "corner composition," defined as the diboride compounds enriched by the transition metals. For example, in the case of Hf rich (HEA_HfB$_2$) with eight transition metal atoms, four are Hf, and the other transition metals will have only one atom each. And each corner's rich composition varied the temperature into three different high temperatures, 3500K, 5000K, and 6000K. With all corners calculated, there are five corner compositions with three temperatures & 5 different volumes. In each case, the atomic position was randomized & vary based on the number of transition metals and the volume sampled. The volumes include the standard volume and 5% and 10% expansion/reduction. Figure 11 is the schematic idea of how to pick the area for DFT calculation. This strategy is called as High Entropy Alloy Strategy.
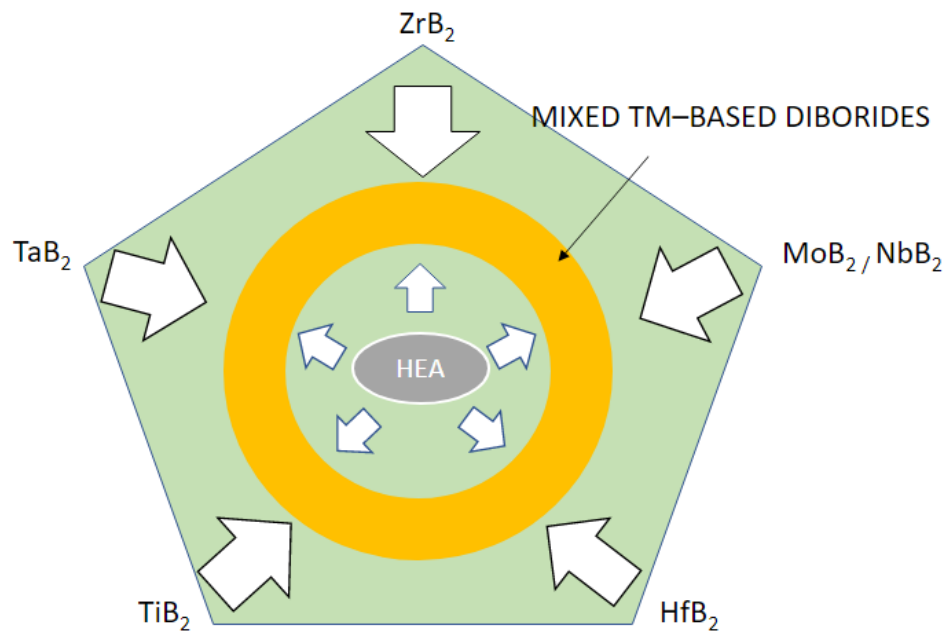
Figure 11. Schematic of HEA Strategy

The other calculation was also done with mixed composition with five different varied compositions, varied randomly for each five transition metals, with sampling with the same temperature and volume as specified in corner-rich above. The other data was produced in relatively low temperatures, 1000K, with five different volumes.

Deep Neural Networks (DeePMD & Allegro Package)

After finishing all calculations and variations that have been done in VASP, the next step is to develop the interatomic potential with the deep learning process. As discussed in the previous chapter, the potential developed used two codes based on deep Learning, DeePMD, and Allegro. Both codes have different preprocessing steps for the vasprun to be able to read as an input for the neural network.

For the DeePMD, after the calculation result (vasprun.xml) is collected from all various compositions, volumes, and temperatures. Then, all vasprun files were shuffled and preprocessed with dpdata based on the Python script. After all mixed data from all vasprun, the result will generate the Deep Data folder, which comes from the shuffled vasprun result and become input for the DeePMD. The next step is to prepare the script for information for DeePMD with *. json script. The script defines all the learning rates, cutoff radius, and stop batch before the fitting process starts. Based on the previous study, some training variable was followed, such as a cutoff radius of 5.8 angstroms, which determined able to capture neighbor interactions of up to the third nearest neighbor from each training [28]. This study uses the dptrain command featured in the DeePMD code. The process of this training is defined as 3500000 steps. Please see Appendix A to see further details of the training input for DeePMD,

In Allegro, the first step is to preprocess the data obtained from vasprun by combining all the vasprun into one data file on *. extxyz file. The combining process is developed using Python script, resulting in all the vasprun.xml files converting to extxyz. In the following procedure, prepare the input file specifying the learning rate, number of layers, cutoff radius, and other variables. Then, the process will start with running the command nequip-train. The training process is limited to 500 epochs. Please refer to Appendix B of this thesis for further information about more detailed training parameters.

Molecular Dynamics Simulation (LAMMPS)

In the last process of the methodology, this study implemented the developed potential (both DeePMD and Allegro) to molecular dynamics simulation, which in this study generated the data using LAMMPS. After training, the process will deploy the model and generate the interatomic potential files.

The DeePMD function to do this process is called the "dp-freeze" process. which deploys the training result into interatomic potential files (*.pb). Then we plot some properties by simulating the elastic and lattice constant, which was already determined per the previous study[29]. In Allegro, the function to develop the potentials after the training process is called "nequip-deploy," which will generate the interatomic potential files for Allegro (*.pth). Allegro and DeePMD have an interface with LAMMPS, specified in the pair style and pair coeff section on LAMMPS input.

RESULTS AND DISCUSSION

DeePMD Interatomic Potentials for High Entropy Diborides

In this study, the total trajectories involved in the analysis were 46,710 for the HEA_MB2_Mo and 36637 for HEA_MB2_Nb. Regarding the data quality, all data were calculated with KPOINTS 3x3x3. In the case of HEA_MB2_Mo, I employed a mixed resolution calculation with ALGO "Normal" and ALGO "Fast" as defined in https://www.vasp.at/wiki/index.php/Input, which boosts the number of trajectories that are used in each material. With low-resolution calculation, the number of trajectories will increase as the calculation is for a given supercomputer computing hour.

To understand the model's accuracy, DeePMD has a feature called dptest which evaluates the model based on the energy, force, and virial. In this study, I utilize this function to evaluate the model of DeePMD. Then compare the data obtained from DFT calculation versus the prediction energy, forces, and virial from DeePMD results. The plot of the graph below, of dptest result from HEA_MB2_Mo, shows the error level of each variable. The result of dptest shows the average Energy RMSE/Natoms is 1.197928e-02 eV, then the force average error is 2.872448e-01 eV/A, and the Virial RMSE/Natoms is 4.962046e-02 eV. The error value shows that the build model of HEA_MB2_Mo has a relatively accurate model in terms of evaluation from energy, forces and virial. Then, the result also indicates that the force had comparatively high error compared to the energy and stress. Figure 12 shows the trend between the DFT calculation result of Energy, Forces (x, y, z), and virial (xx, yy, zz) compared with the Prediction from DeePMD.

(a)

(b)

(c)
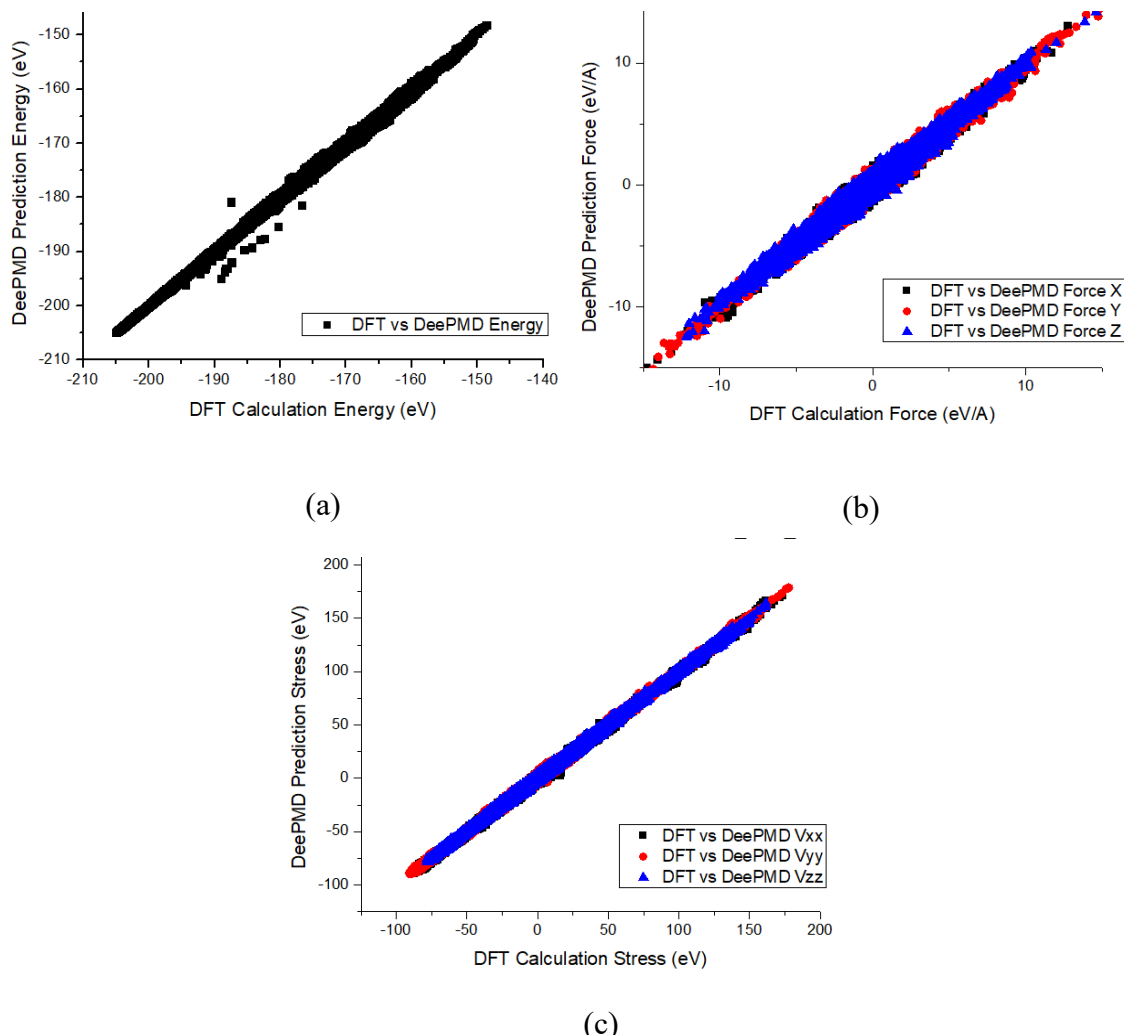
Figure 12. Evaluation of DeePMD, comparison between (a) DFT Calculation vs. DeePMD Prediction of energy, (b) force, (c) virial, Model for HEA_MB2_Mo with DPTEST function

The HEA_MB2_Mo results were compared with those from HEA_MB2_Nb as shown in Figure 13, which use more accurate calculation (high-resolution data); the DeePMD result of the dptest function generated the error value of this model. This study got the error value for the Energy RMSE/Natoms as 9.677641e-03 eV, while the Force RMSE and Virial RMSE/Natoms are 2.866047e-01 eV/A and 4.660441e-02 eV, respectively, with a smaller number of systems, 263 calculations.

(a)

(b)

(c)
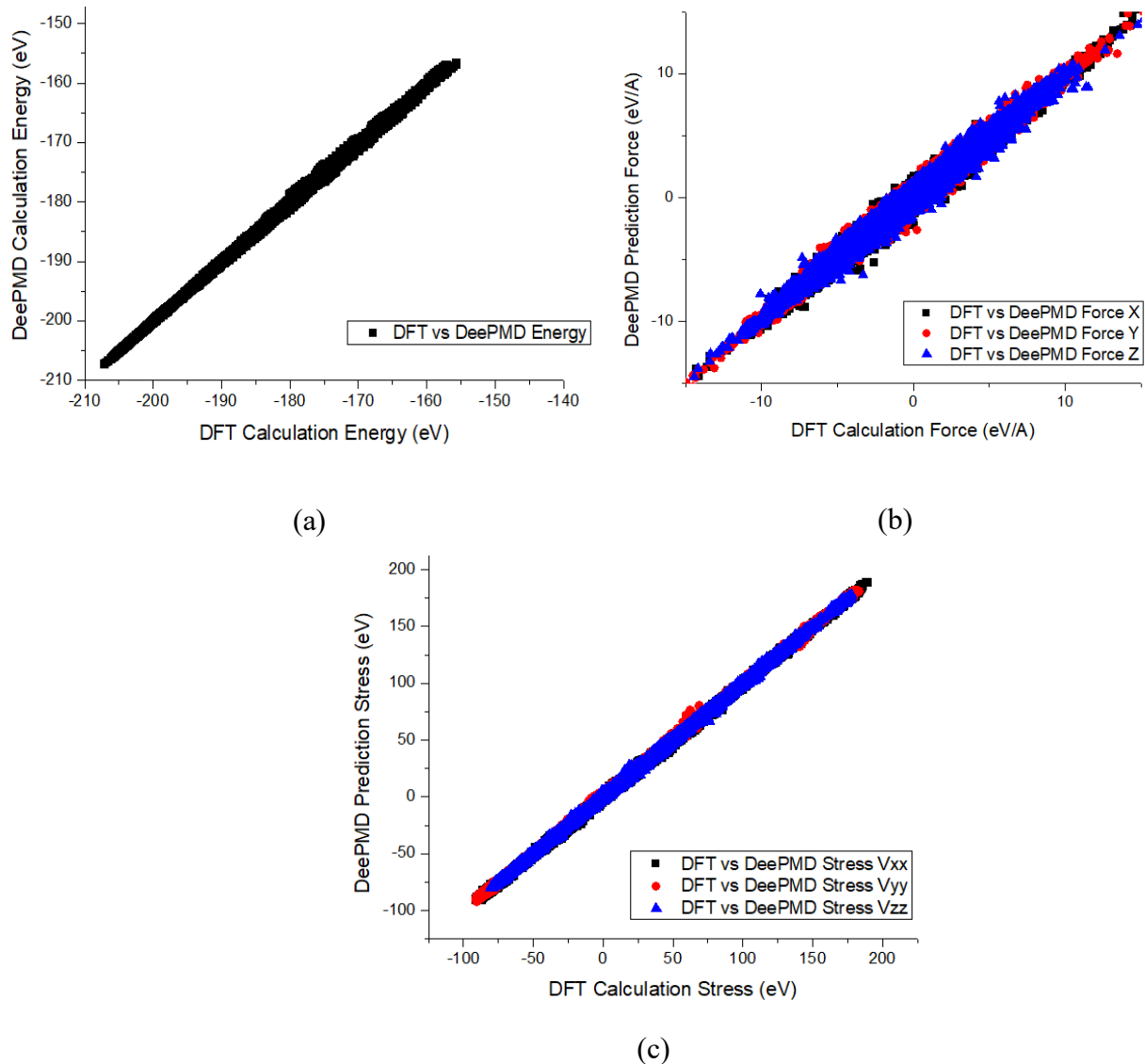
Figure 13. Evaluation of DeePMD, comparison between (a) DFT Calculation vs. DeePMD Prediction of energy, (b) force, (c) virial, Model for HEA_MB2_Nb with DPTEST function

Simulation of DeePMD Interatomic Potentials on Molecular Dynamics

One of the aims of this study is to generate potential models that can withstand elevated temperatures as per real applications. Then, to understand the stability of this model, I try to plot the response of the lattice constant toward temperature. The built model is then interfaced with the molecular dynamic simulation, LAMMPS. In this simulation, this study utilizes NPT

ensembles by increasing the temperature from 300K to 2000 K, then plotting the lattice constant

vs. temperature, which can be seen in Figure 14.
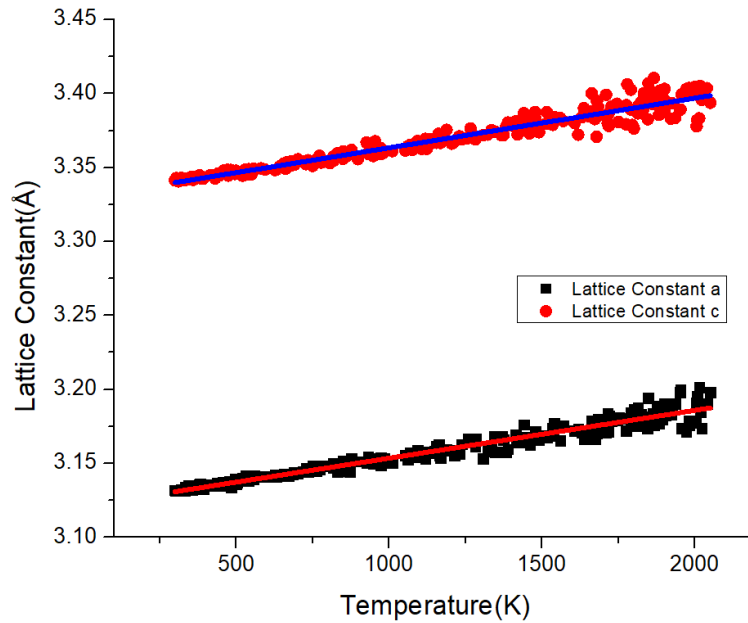
(a)
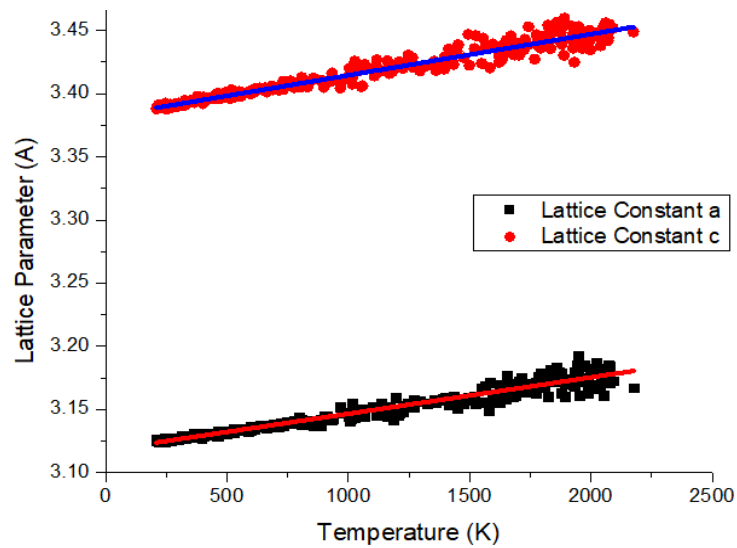
(b)

Figure 14. Evaluation of Lattice constant on temperature for (a) High Entropy Diboride
Molybdenum (b) High Entropy Diboride Niobium, in the range 300 K to 2000 K

The lattice constant graph shows that the lattice parameter for the HEA_MB2_Mo and HEA_MB2_Nb slightly increase while expanding along the temperature. In 300K, the lattice constant a is for HEA_MB2_Mo and HEA_MB2_Nb are 3.13 & 3.14 angstrom. The constant lattice c for the HEA_MB2_Mo and HEA_MB2_Nb are 3.34 & 3.38 angstrom. On the temperature 2000K, the lattice a of HEA_MB2_Mo and HEA_MB2_Nb expand to 3.16 and 3.18 angstrom, while on the lattice constant c expansion to 3.40 and 3.44 angstrom for HEA_MB2_Mo and HEA_MB2_Nb, respectively.

Both results were consistent with the result obtained from the experiment by Gild (2016) [8], which found in room temperature, the lattice constant of HEA_MB2_Mo is 3.097 and 3.307 for lattice constant a and c, respectively. And for the lattice constant a and c for HEA_MB2_Nb is 3.11 and 3.346 angstrom.

As discussed in the introduction chapter, one target for developing interatomic potential is to capture more significant areas of the composition. And in this case, it becomes beneficial for the development of interatomic potential for high entropy diboride to capture not only as five element system but also back to a binary system. In this case, this study tried the transferability of our potential by applying this to each binary system.

The study tried each binary's elastic constant, HfB2, ZrB2, TaB2, NbB2, MoB2, and TiB2, which method based on the script has been published [30] and compared the result obtained based on other methods, such as molecular dynamics and first principles [31-34] and based on materials database [35-38] which determined on a different method. This study then ran each LAMMPS to simulate the binary's elastic constant (Cij) and compared it with the data from the previous study. For the HfB2, this study found that the bulk modulus for our model got 290 GPa, while the previous study found that HfB2 has a bulk modulus of 248 GPa [31], while the

other study found a bulk modulus of 272 GPa [35]. The other result for HfB2 found that the C11, C33, and C44 can model the elastic constant with the result on 604 GPa, 443, and 237 GPa, respectively. The summary of the Cij value can be found in Table 2 as follows. On the ZrB2, this potential model found the bulk modulus 269 GPa, slightly higher than the reference, 240 GPa [36]. It also found that C11 matched well with the reference [32] with only 1 GPa off. The C12 on this model is relatively higher than the reference; while the reference found 61 GPa, the model found the value of C12 is 107 GPa. The TaB2 model also found that the Poisson ratio of 0.20 matched well with the previous work's 0.21 [33], and the bulk modulus of TiB2 also can capture a close value to the previous work, with 256 Gpa [34] while this study found 243 GPa.

Table 2. Evaluation of Elastic constant of Binary System for HEA_MB2_Mo

TM-Diboride	C11 (GPa)	C12 (GPa)	C13 (GPa)	C33 (GPa)	C44 (GPa)	Poisson ratio	Bulk Modulus (GPa)
HfB$_2$	604	113	177	443	237	0.21	290
Reference [31]	608	73	135	468	272	0.14	248
Reference [35]	594	65	125	448	262	0.13	272
ZrB$_2$	566	107	157	447	240	0.21	269
Reference [32]	567	56	120	436	247	0.13	240
Reference [36]	553	61	123	428	246	0.14	238
TaB$_2$	532	98	146	403	212	0.20	248
Reference [33]	598	145	214	443	208	0.21	308
Reference [37]	593	148	196	461	209	0.23	303
TiB$_2$	556	92	106	421	246	0.17	243
Reference [34]	699	57	95	467	265	0.10	256
Reference [38]	642	75	106	443	258	0.13	256

On the HEA_MB2_Nb Potential, which the result can be shown in Table 3, the elastic constant value on each binary system is improving compared to the previous model. While

modeling the elastic constant of HfB2, This research found the result on Bulk Modulus on 234 GPa, while based on previous work found quite match well with 248 [31]. The Poisson ratio on 0.18 and C11, C33, and C44 is 525, 383, and 218 GPa. In the ZrB2 model, I found the potential to match well with the reference [36]. The Bulk modulus is only shifted lower by 6 GPa with the reference 232 GPa [36]. The other value also shifted only below 1%, with the C11. C33 and C44 are 531, 396, and 234 GPa. For the TiB2, the C11 value shifted relatively high compared to the reference, which found 642 GPa[38], while the other value was very close.

Table 3. Evaluation of Elastic constant of Binary System for HEA_MB2_Nb

TM-Diboride	C11 (GPa)	C12 (GPa)	C13 (GPa)	C33 (GPa)	C44 (GPa)	Poisson ratio	Bulk Modulus (GPa)
HfB$_2$	525	94	112	383	218	0.18	234
Reference [31]	608	73	135	468	272	0.14	248
Reference [35]	594	65	125	448	262	0.13	272
ZrB$_2$	531	88	112	396	234	0.17	232
Reference [32]	567	56	120	436	247	0.13	240
Reference [36]	553	61	123	428	246	0.14	238
TaB$_2$	543	89	114	365	214	0.18	231
Reference [33]	598	145	214	443	208	0.21	308
Reference [37]	593	148	196	461	209	0.23	303
TiB$_2$	627	118	183	495	275	0.21	301
Reference [34]	699	57	95	467	265	0.10	256
Reference [38]	642	75	106	443	258	0.13	256

Another significant result obtained in this research is to simulate the melting process of the high entropy diborides-Niobium and high entropy diborides-molybdenum used to simulate the ZrB2 melting process. With a similar approach, this study utilizes the developed interatomic potentials to simulate the melting temperature of the high entropy materials.

The study also simulates the interatomic potential developed from DeePMD and utilizes the LAMMPS with the NPT function. The simulation increased its temperature from 300K and then increased it to 6000K. From the result of the LAMMPS, it obtained the data of temperature vs. volume. The graph below shows that at a specific temperature, the expansion of the volume increased significantly, which can be seen as the signal of the phase change (phase transition). In the HEA_MB2_Mo potential, it can be seen that the temperature where the volume changes notable change is ~3300K. The result of the melting process plot can be found in Figure 15.
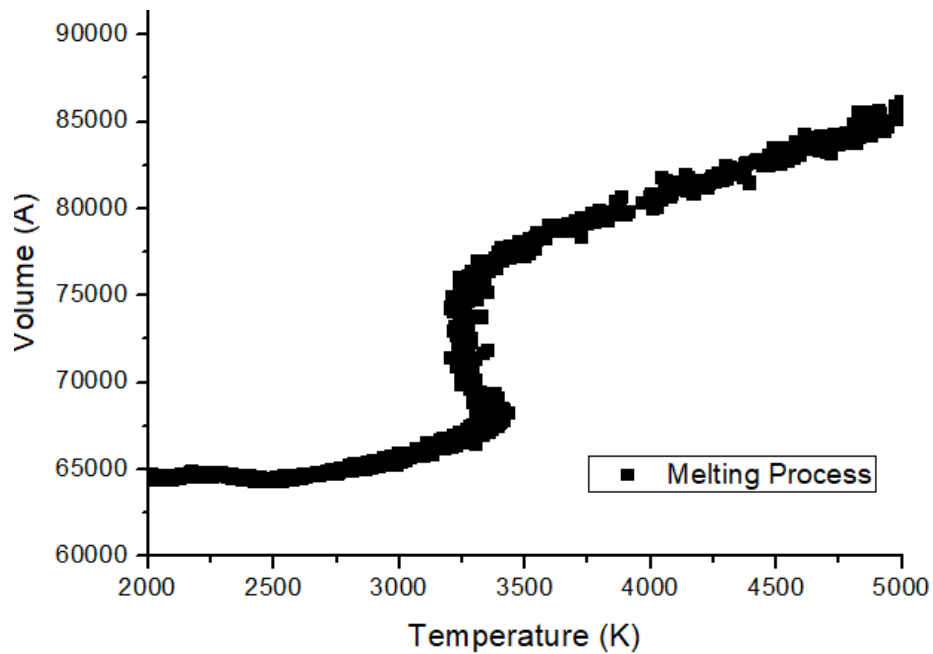
Figure 15. The plot from the LAMMPS result of the Melting Process for the HEA_MB2_Mo interatomic potentials, with plot Temperature vs. Volume on NPT function

Based on the study obtained from the LAMMPS result for the HEA_MB2_Nb interatomic potentials, I found that the transition temperature on this result is slightly shifted to ~3500K with the same set of our LAMMPS model.

This research's sample drives the shifting of HEA_MB2_Nb potential. In the

HEA_MB2_Mo, the potential is developed using the MoB2, which has a melting point of

~2500K. In the HEA_MB2_Nb, I developed the Potential with NbB2, which has a melting point

of ~3000K. The result of this LAMMPS simulation can be seen in the plot in Figure 16.
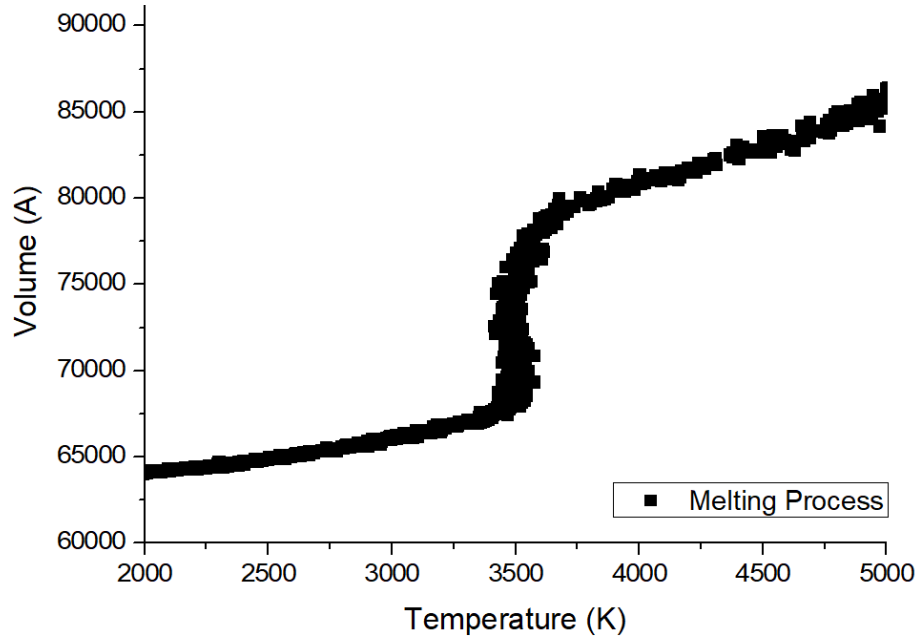
Figure 16. The plot from the LAMMPS result of the Melting Process for the HEA_MB2_Nb
interatomic potentials, with plot Temperature vs. Volume on the NPT function

This study tries to optimize specifically for ZrB2. The other properties that I tried to

model with both potentials are the vibration characteristics which will reflect in the phonon

dispersion curve on ZrB2. The Phonon dispersion curve that I obtained comes from a code called

Alamode [39]. The mass of the ZrB2 is in between other constituents on our high entropy model,

which should give an idea about the average trend of the vibrational characteristics from the

developed potentials on each element. Each potential found can give an expected trend on the

vibrational characteristics for ZrB2 then the result is compared to the curve obtained from DFT

and other published references [40]. The result of the Phonon Dispersion curves can be found in Figure 17.

<div align="center">(a)   (b)</div>
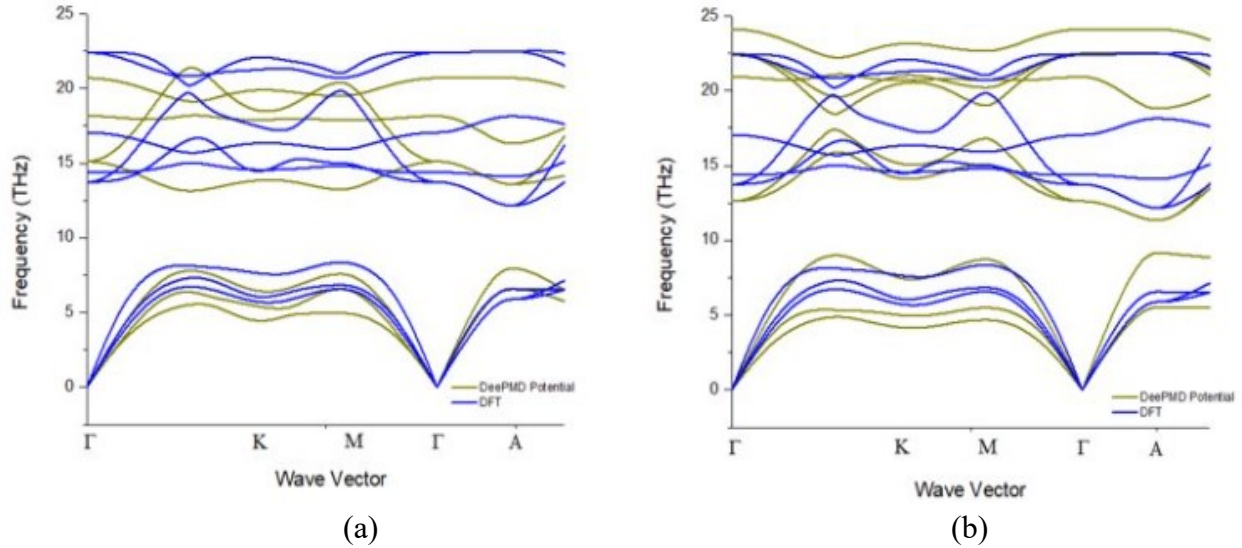
Figure 17. Phonon Dispersion of ZrB2 from DeePMD Potential Result vs. DFT calculation result from (a) HEA_MB2_Mo Potential (b) HEA_MB2_Nb Potential

Interestingly, in the optical mode, the HEA_MB2_Nb can give better results than the HEA_MB2_Mo, which this study assumes is because the increment in our data accuracy helps refine the data. On the other hand, in the acoustic mode, both potentials can match well, with comparatively the HEA_MB2_Mo having a better curve. In this aspect, the increment in our data trajectory on this potential helps us better resolve the transition metal vibration.

Allegro Interatomic Potential for High Entropy Diborides

In this section, the evaluation of the Potential development from Allegro code was discussed by comparing the result obtained from the DFT calculation and the Prediction obtained from Allegro. To obtain the energy and force predicted by Allegro, I use the nequip-evaluate function. Then this study gets all the predicted energy and force. Figure 18 shows the plot result from DFT vs. Allegro results for HEA_MB2_Mo.
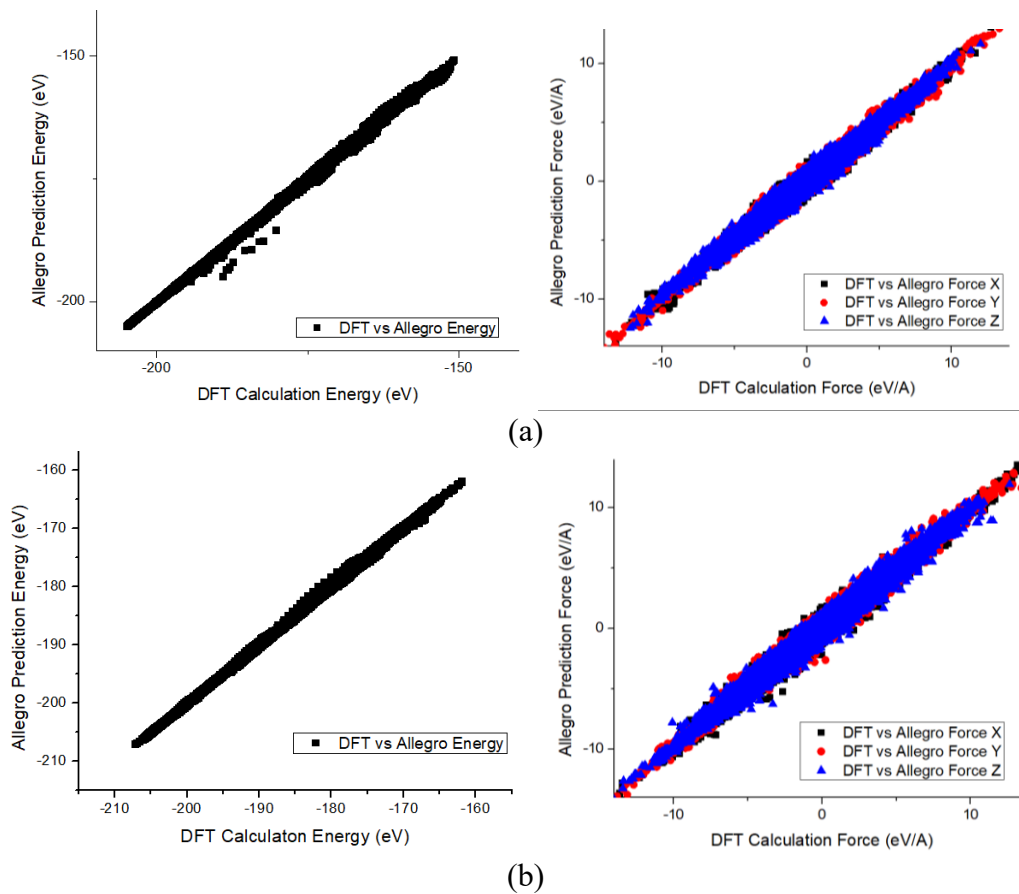
Figure 18. Evaluation of DeePMD, comparison between (a) DFT Calculation vs. Allegro Prediction of energy and force for Model for HEA_MB2_Mo (b) DFT Calculation vs. Allegro Prediction of energy and force for Model for HEA_MB2_Nb, with nequip-evaluate function

This study also tries to optimize the variable of our training by running the same dataset with a different learning rate (LR), number of the neural network layer (L), and cutoff radius. The analysis is then obtained from the Weight and Biases portal, which interfaces with Allegro to analyze the data obtained from the training process. The first result tried to see the effect of those variables on the energy and force validation of our training.

In this study also compares training with allegro code based on different hyperparameters on HEA_MB2_Mo data. The energy plot and force plot shown that the energy and force

validation reach 0.003 eV/A and 013 eV/A, respectively, at a learning rate of 0.001 with the

cutoff radius of 6 Angstrom and the number of layers at eight layers. The result can be found on

Figure 19.
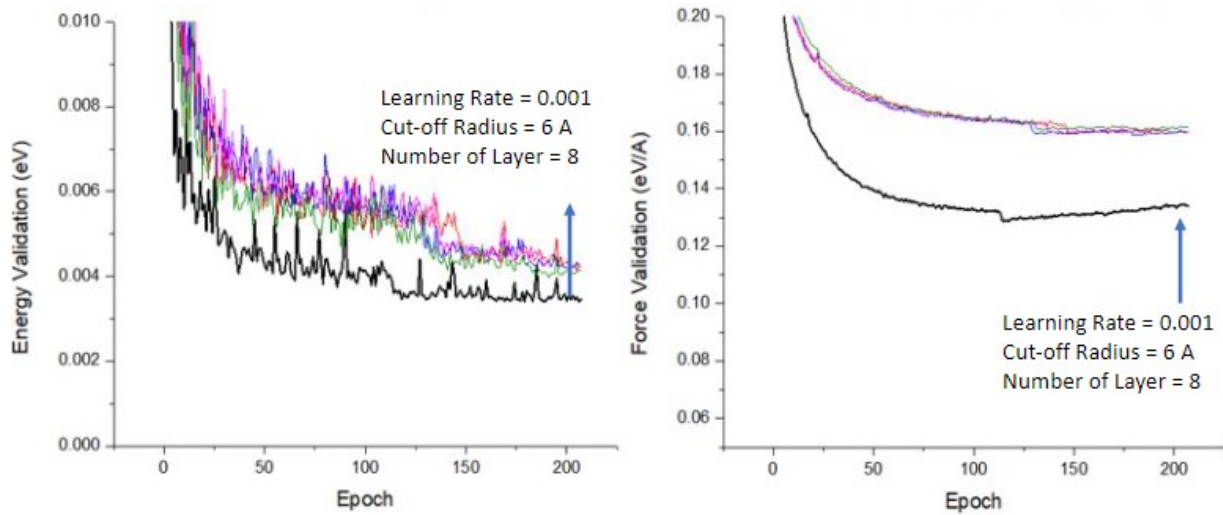
Figure 19: Evaluation of Hyperparameter to energy and force validation for HEA_MB2_Mo
Allegro Interatomic Potential by varying the Learning Rate (LR), number of Layer (L), and
cutoff radius (RAD)

In Figure 20, the hyperparameter effect on energy and force validation for

HEA_MB2_Nb, this study found that the learning rate of 0.0005 with the number of layers (L)

set to 8 and cutoff radius 6 Angstrom, can give the best model, with the energy and force

validation reach 0.0020 eV/A and 0.7 eV/A, respectively. This result then analyzes further with

the parallel plot of each hyperparameter to see the effect of the training error on both potentials.
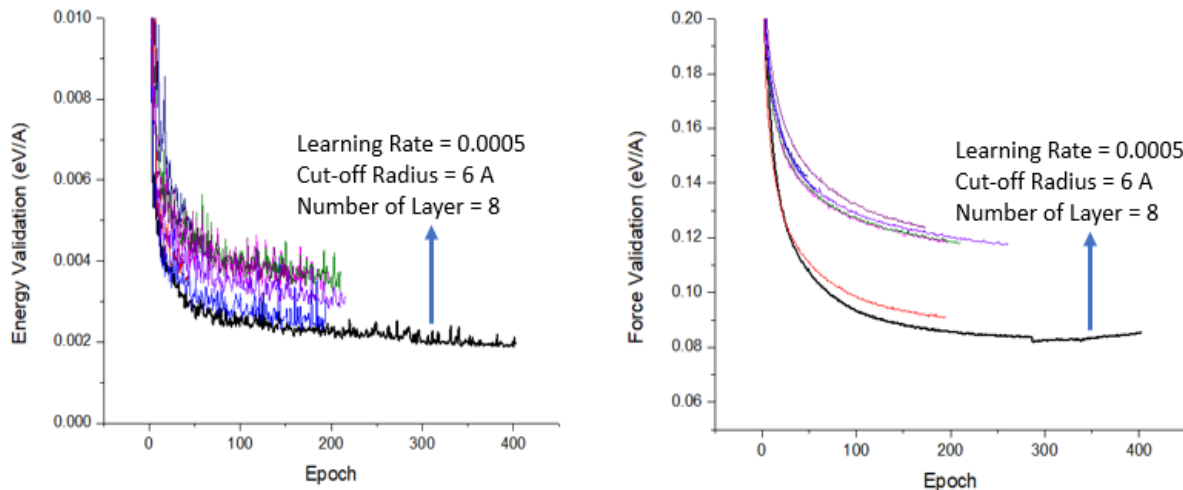
Figure 20. Evaluation of Hyperparameter to energy and force validation for HEA_MB2_Nb Allegro Interatomic Potential by varying the Learning Rate (LR), number of Layer (L), and cutoff radius (RAD)

The following result shows the plot of three variables significantly affects the training error. In Figure 21 (a), which shows the hyperparameter effect towards HEA_MB2_Mo, this study found that the medium learning rate at 0.001 will give the lowest error in the low-quality data(HEA_MB2_Mo). On the other hand, the maximum cutoff radius at 6.0 Angstrom and the highest layer number at eight layers give the lowest error of the trained model. On the other hand, the result of HEA_MB2_Nb, as depicted in Figure 21 (b), shows the cutoff radius and total layer. At the same time, the lowest learning rate at 0.0005 will significantly impact the error from our training result. In contrast, with the other hyperparameter variables, cutoff radius, and the number of layers, the result on high-quality data shows the same effect as the low-quality data.
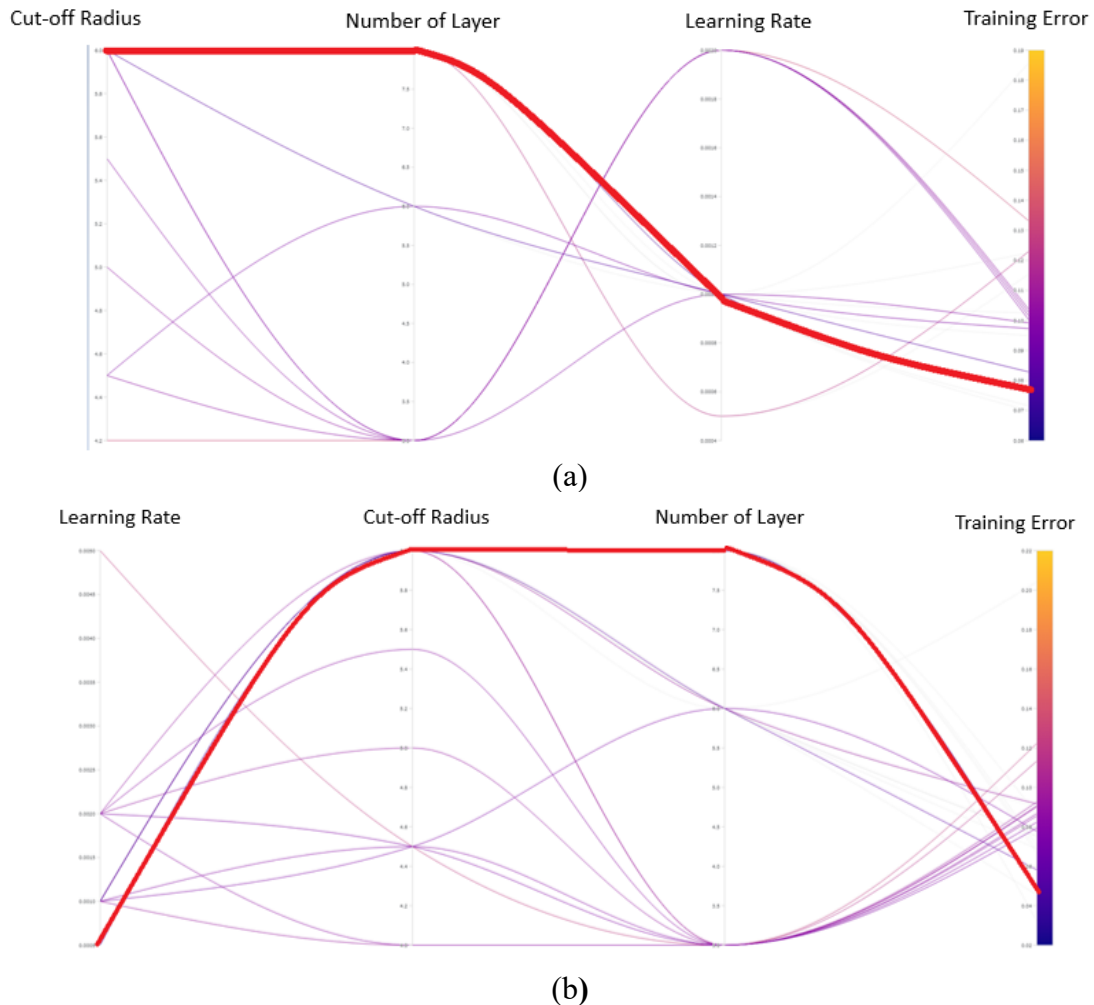
Figure 21. Evaluation of Hyperparameter effect for Training Error on development of Allegro Interatomic Potential (a) HEA_MB2_Mo (b) HEA_MB2_Nb, by varying the Learning Rate (LR), number of Layer (L) and cutoff radius (RAD).

The next segment also gives us better diagnostics of the data employed for this study and their accuracy. Allegro can assess the quality of our Prediction for each element. Such a detailed evaluation provides a better guide on refining our next training by focusing, for example, on those that exhibit less desirable accuracy.

The following result compares the accuracy of the validation sets of the data from HEA_MB2_Mo versus HEA_MB2_Nb. It found that Niobium and Molybdenum atoms contribute to the highest validation error compared to the rest of the constituents of MB2. The

exciting result below can relate to the phonon dispersion plot on the DeePMD result. As noted, the HEA_MB2_Mo has an issue with the higher frequency, which the Boron drives. The validation results above showed that the data validation on boron elements tends to plateau on the HEA_MB2_Mo, which indicates that the error is in line with the result with the phonon result on DeePMD. From this, this study can identify that the data sampling on Boron for our HEA_MB2_Mo has lower accuracy. The detailed result of each element plot can be found in Figure 22.

(a)

(b)
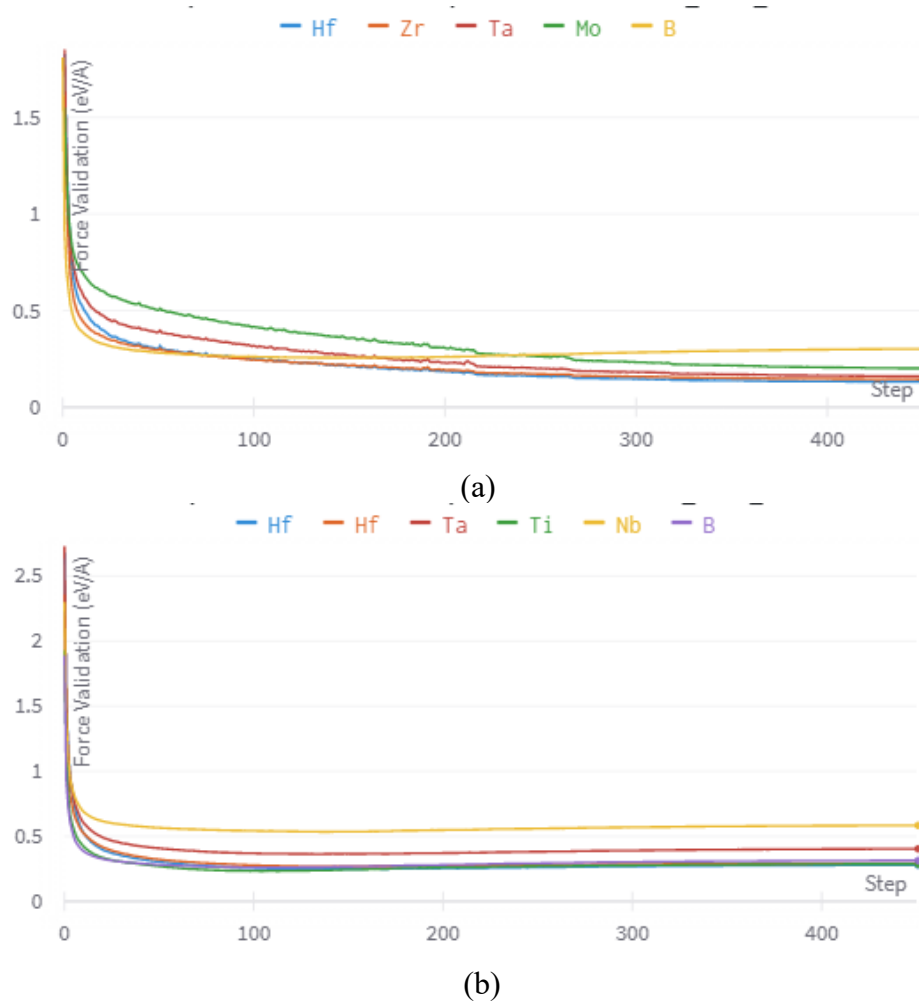
Figure 22. Step vs. Force Validation on (a) HEA_MB2_Mo (b) HEA_MB2_Nb, taken per constituent on materials.

Simulation of Allegro Interatomic Potentials on Molecular Dynamics

This study focuses on how the response of interatomic potential can show the stability of the materials at elevated temperatures, which tested at two elevated temperatures is done to understand the response of the materials at elevated temperatures. In this section, the testing on interatomic potentials which develop through Allegro was being tested on the molecular dynamics simulation, LAMMPS. The radial function distribution analysis at 1000K and 2000K, as shown in Figure 23, proved that at each temperature, the potential ability to remain stable in the crystal form.

(a)

(b)
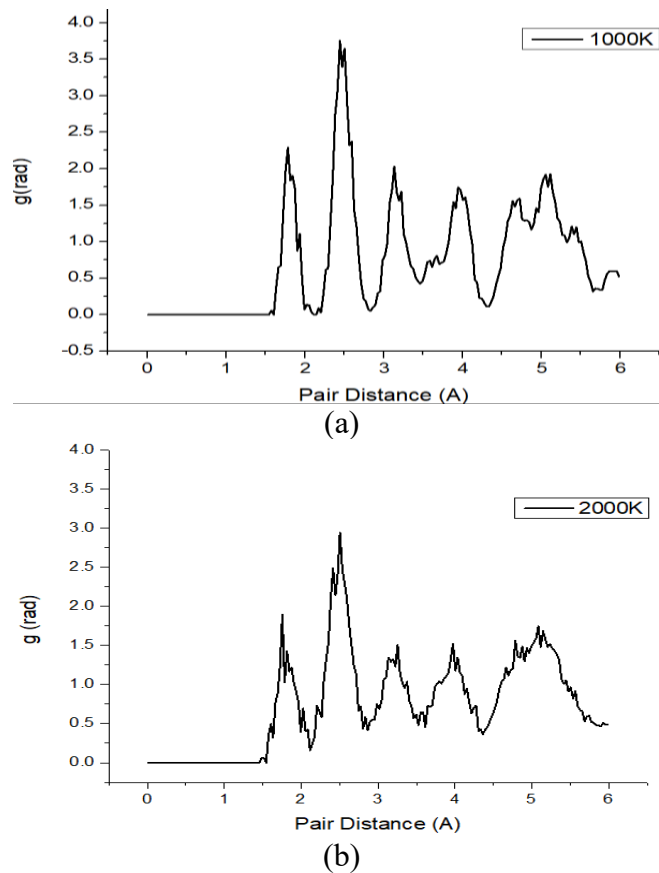
Figure 23. Radial Distribution Function Analysis on (a) 1000K (b) 2000K temperatures for HEA_MB2_Nb

The stability of the crystal structure at 2000K, as shown in Figure 24, verifies that this material's MD (Molecular Dynamics) simulation using the Allegro-generated Potential can withstand the elevated temperature. This result is consistent with the experimental findings of UCSD's group, which synthesized the same composition through an ultra-high temperature sintering process up to 2000°C [8].
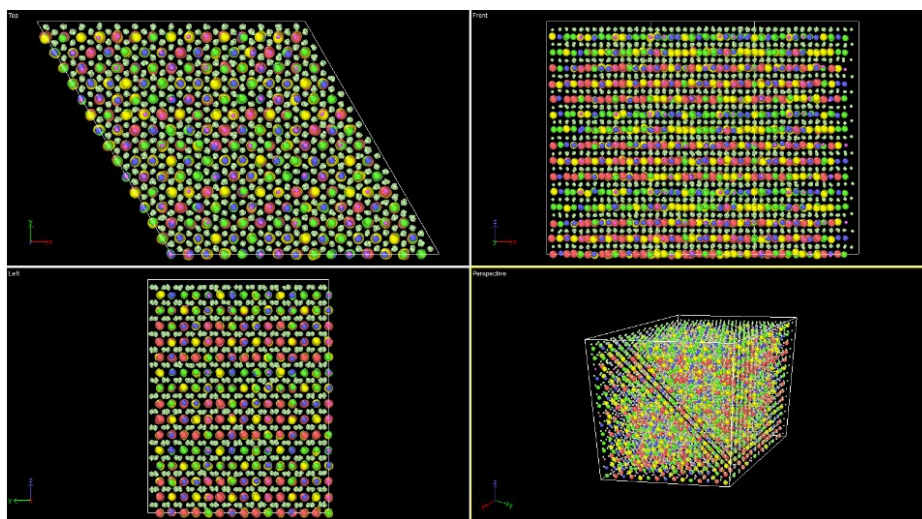
Figure 24. Stability test with NVT function of Allegro Potential on 2000K

Comparison Study of DeePMD and Allegro Interatomic Potential

The last section of the result compares what this study got on DeePMD interatomic potential with the work result on Allegro Potential. As noted, both codes have different approaches to decomposing energy formalism and how the DeePMD focuses on invariant descriptors based on scalar. In contrast, Allegro combines both the scalar and the equivariant descriptors. As discussed in the introduction of about five interatomic potential aspects, This study intends to compare these two codes based on the accuracy level and the computational efficiency.

The following results compare the accuracy between the two potentials by evaluating the RMSE of the model for HEA_MB2_Nb, for the energy and forces, respectively, as a function of the steps. The original DeePMD data were calculated with steps. In contrast, the Allegro data were calculated with epoch. I convert the data into steps to give the same scale for the two methods.

Figure 25 shows that Allegro could give a higher accuracy than DeePMD. In the case of energy comparison, this study found that both methods show a similar level of accuracy. It is worth noting, however, that beyond the 20000 steps, Allegro results in better accuracy.
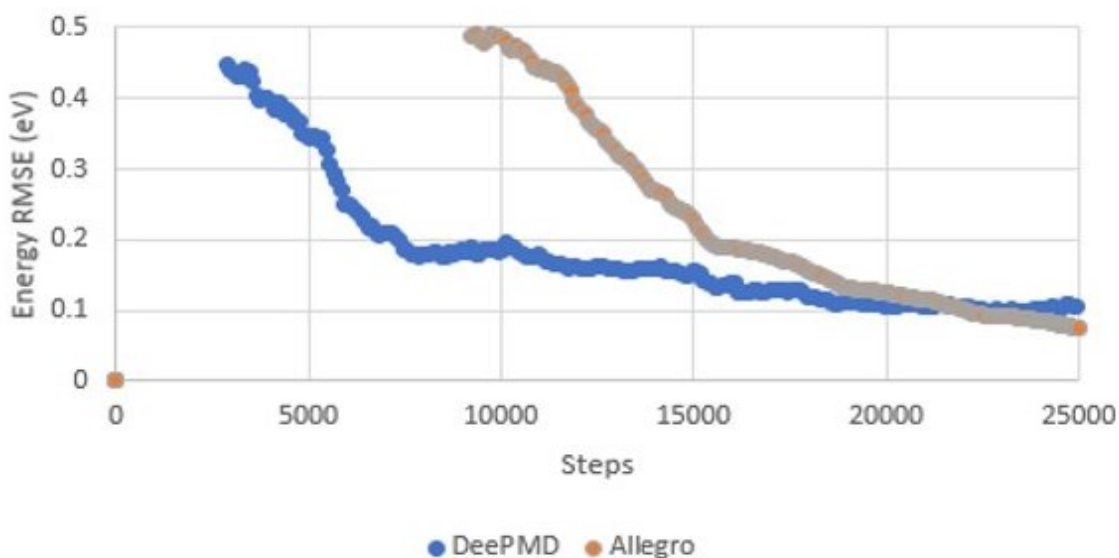
Figure 25. Computational Steps vs. Accuracy of Developed Interatomic Potentials from DeePMD vs. Allegro Energy RMSE

In the force comparison, the Allegro achieved much higher accuracy throughout the steps. The use of tensors, in this case, seems to help significantly in reducing the error level. It can capture the fundamental physics behind the force balance calculation result, consistent with the DFT calculations. Overall, both approaches provide a satisfactory level of accuracy. Allegro

excels with more steps, especially concerning its energy predictions. The result, which is shown

in Figure 26, may be caused by the added complexity (the inclusion of the tensorial products) of

the structure of the Deep Learning model within Allegro.
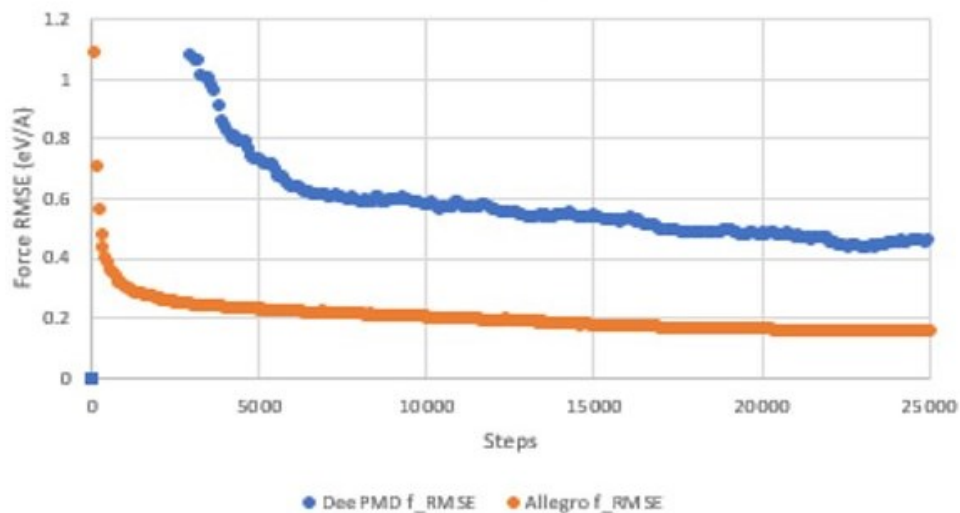
Figure 26. Computational Steps vs. Accuracy of Developed Interatomic Potentials from DeePMD vs. Allegro Force RMSE

CONCLUSION

The High Entropy Diborides, interatomic potential with machine learning, and neural networks were developed using the High Entropy Alloy Strategy. Optimizing the corner composition calculation and sampling in five elements component system is a very efficient and effective way to sample the high entropy alloy interatomic potential development through two machine learning interatomic potential codes, DeePMD and Allegro.

The strength of the DeePMD, with the excellent accuracy of energy, forces, and viral Prediction, is also obtained in this study. The interface of interatomic potential to molecular dynamics simulation to model and compare with the result from the experiment is also being demonstrated with compare with the stability on elevated temperature. The transferability of the potential is also demonstrated in this study.

The Allegro result also showed a promising result, demonstrating incredibly low error and good accuracy on the developed model. The strength of Allegro by implementing the scalar and tensor combination on the code can optimize the force error compared to the result obtained from DeePMD results.

In the future, combining this result and implementing Active learning is an up-and-coming technique to refine the obtained result. The active learning will be able to identify the bad data, which later can automatically produce the refined calculated data, which promises not only to increase the accuracy but also good for reducing the number of samples and computational efficiency.

REFERENCES

[1] J. Gild, A. Wright, K. Quiambao-Tomko, M. Qin, J.A. Tomko, M. Shafkat bin Hoque, J.L. Braun, B. Bloomfield, D. Martinez, T. Harrington, K. Vecchio, P.E. Hopkins, J. Luo, Thermal conductivity, and hardness of three single-phase high-entropy metal diborides fabricated by borocarbothermal reduction and spark plasma sintering, Ceramics International 46(5) (2020) 6906-6913.

[2] W.G. Fahrenholtz, G.E. Hilmas, I.G. Talmy, J.A. Zaykoski, Refractory Diborides of Zirconium and Hafnium, Journal of the American Ceramic Society 90(5) (2007) 1347-1364.

[3] V. Mazánek, H. Nahdi, J. Luxa, Z. Sofer, M. Pumera, Electrochemistry of layered metal diborides, Nanoscale 10(24) (2018) 11544-11552.

[4] H. Yuan, Z. Li, J. Yang, Transition-Metal Diboride: A New Family of Two-Dimensional Materials Designed for Selective CO_2 Electroreduction, The Journal of Physical Chemistry C 123(26) (2019) 16294-16299.

[5] M.-H. Tsai, J.-W. Yeh, High-Entropy Alloys: A Critical Review, Materials Research Letters 2(3) (2014) 107-123.

[6] Y. Zhang, T.T. Zuo, Z. Tang, M.C. Gao, K.A. Dahmen, P.K. Liaw, Z.P. Lu, Microstructures and properties of high-entropy alloys, Progress in Materials Science 61 (2014) 1-93.

[7] B. Cantor, Multicomponent and High Entropy Alloys, Entropy 16(9) (2014) 4749-4768.

[8] J. Gild, Y. Zhang, T. Harrington, S. Jiang, T. Hu, M.C. Quinn, W.M. Mellor, N. Zhou, K. Vecchio, J. Luo, High-Entropy Metal Diborides: A New Class of High-Entropy Materials and a New Type of Ultrahigh Temperature Ceramics, Scientific Reports 6(1) (2016) 37946.

[9] N. Mardirossian, M. Head-Gordon, Thirty years of density functional theory in computational chemistry: an overview and extensive assessment of 200 density functionals, Molecular Physics 115(19) (2017) 2315-2372.

[10] J.S. Tse, AB INITIO MOLECULAR DYNAMICS WITH DENSITY FUNCTIONAL THEORY, Annual Review of Physical Chemistry 53(1) (2002) 249-290.

[11] D. Zhou, An Introduction of Density Functional Theory and its Application, 2008.

[12] J. Behler, M. Parrinello, Generalized Neural-Network Representation of High-Dimensional Potential-Energy Surfaces, Physical Review Letters 98(14) (2007) 146401.

[13] J. Behler, Perspective: Machine learning potentials for atomistic simulations, The Journal of Chemical Physics 145(17) (2016) 170901.

[14] P.E. Dolgirev, I.A. Kruglov, A.R. Oganov, Machine learning scheme for fast extraction of chemically interpretable interatomic potentials, AIP Advances 6(8) (2016) 085318.

[15] N. Artrith, J. Behler, High-dimensional neural network potentials for metal surfaces: A prototype study for copper, Physical Review B 85(4) (2012) 045439.

[16] M. Gastegger, P. Marquetand, High-Dimensional Neural Network Potentials for Organic Reactions and an Improved Training Algorithm, Journal of Chemical Theory and Computation 11(5) (2015) 2187-2198.

[17] G.P.P. Pun, R. Batra, R. Ramprasad, Y. Mishin, Physically informed artificial neural networks for atomistic modeling of materials, nature Communications 10(1) (2019) 2339.

[18] J.S. Smith, O. Isayev, A.E. Roitberg, ANI-1: an extensible neural network potential with DFT accuracy at force field computational cost, Chemical Science 8(4) (2017) 3192-3203.

[19] L. Zhang, J. Han, H. Wang, R. Car, W. E, Deep Potential Molecular Dynamics: A Scalable Model with the Accuracy of Quantum Mechanics, Physical Review Letters 120(14) (2018) 143001.

[20] N. Lubbers, J.S. Smith, K. Barros, Hierarchical modeling of molecular energies using a deep neural network, The Journal of Chemical Physics 148(24) (2018) 241715.

[21] K. Schütt, P.-J. Kindermans, H.E.S. Felix, S. Chmiela, A. Tkatchenko, K.-R. Müller, SchNet: A continuous-filter convolutional neural network for modeling quantum interactions, NIPS (2017)

[22] H. Wang, L. Zhang, J. Han, E. Weinan, DeePMD-kit: A deep learning package for many-body potential energy representation and molecular dynamics, Computer Physics Communications 228 (2018) 178-184.

[23] A.P. Thompson, H.M. Aktulga, R. Berger, D.S. Bolintineanu, W.M. Brown, P.S. Crozier, P.J. in 't Veld, A. Kohlmeyer, S.G. Moore, T.D. Nguyen, R. Shan, M.J. Stevens, J. Tranchida, C. Trott, S.J. Plimpton, LAMMPS - a flexible simulation tool for particle-based materials modeling at the atomic, meso, and continuum scales, Computer Physics Communications 271 (2022) 108171.

[24] A. Musaelian, S. Batzner, A. Johansson, L. Sun, C.J. Owen, M. Kornbluth, B. Kozinsky, Learning local equivariant representations for large-scale atomistic dynamics, Nature Communications 14(1) (2023) 579.

[25] S. Batzner, A. Musaelian, L. Sun, M. Geiger, J.P. Mailoa, M. Kornbluth, N. Molinari, T.E. Smidt, B. Kozinsky, E(3)-equivariant graph neural networks for data-efficient and accurate interatomic potentials, nature Communications 13(1) (2022) 2453.

[26] I.S. Novikov, K. Gubaev, E.V. Podryabinkin, A.V. Shapeev, The MLIP package: moment tensor potentials with MPI and active learning, Machine Learning: Science and Technology 2(2) (2021) 025002.

[27] A. Stukowski, Visualization, and analysis of atomistic simulation data with OVITO–the Open Visualization Tool, Modelling and Simulation in Materials Science and Engineering 18(1) (2010) 015012.

[28] T. McGilvry-James, B. Timalsina, M.M. Mou, R. Sakidja, Deep potential development of transition-metal-rich carbides, MRS Advances 7(22) (2022) 468-473.

[29] F.-Z. Dai, Y. Sun, B. Wen, H. Xiang, Y. Zhou, Temperature Dependent Thermal and Elastic Properties of High Entropy (Ti0.2Zr0.2Hf0.2Nb0.2Ta0.2)B2: Molecular Dynamics Simulation by Deep Learning Potential, Journal of Materials Science & Technology 72 (2021) 8-15.

[30] M. de Jong, W. Chen, T. Angsten, A. Jain, R. Notestine, A. Gamst, M. Sluiter, C. Krishna Ande, S. van der Zwaag, J.J. Plata, C. Toher, S. Curtarolo, G. Ceder, K.A. Persson, M. Asta, Charting the complete elastic properties of inorganic crystalline compounds, Scientific Data 2(1) (2015) 150009.

[31] H. Liang, W. Sun, X. Li, H. Chen, S. Guan, P. Liu, Q. Wang, X. Li, D. He, F. Peng, Study of the compression behavior and elastic properties of HfB2 ceramics using experimental method and first-principles calculations, Journal of Alloys and Compounds 808 (2019) 151764.

[32] N.L. Okamoto, M. Kusakari, K. Tanaka, H. Inui, S. Otani, Anisotropic elastic constants and thermal expansivities in monocrystal CrB2, TiB2, and ZrB2, Acta Materialia 58(1) (2010) 76-84.

[33] W.J. Zhao, Y.X. Wang, Structural, mechanical, and electronic properties of TaB2, TaB, IrB2, and IrB: First-principle calculations, Journal of Solid State Chemistry 182(10) (2009) 2880-2886.

[34] H.Y. Wang, F.Y. Xue, N.H. Zhao, D.J. Li, First-Principles Calculation of Elastic Properties of TiB2 and ZrB2, Advanced Materials Research 150-151 (2011) 40-43.

[35] The Materials Project. Materials Data on HfB2 by Materials Project. United States. doi:https://doi.org/10.17188/1195124

[36] The Materials Project. Materials Data on ZrB2 by Materials Project. United States. doi:https://doi.org/10.17188/1190849

[37] The Materials Project. Materials Data on TaB2 by Materials Project. United States: N. p., 2020. Web. doi:10.17188/1187553.

[38] The Materials Project. Materials Data on TiB2 by Materials Project. United States. doi:https://doi.org/10.17188/1187840

[39] T. Tadano, Y. Gohda, S. Tsuneyuki, Anharmonic force constants extracted from first-principles molecular dynamics: applications to heat transfer simulations, Journal of Physics: Condensed Matter 26(22) (2014) 225402.

[40] E. Deligoz, K. Colakoglu, Y.O. Ciftci, Phonon dispersion and thermodynamical properties in ZrB2, NbB2, and MoB2, Solid State Communications 150(9) (2010) 405-410.

APPENDICES

Appendix A: Input File of DeePMD

```
{   "_comment": " model parameters",

  "model": {
    "type_map":     ["Hf", "Zr", "Ta", "Mo", "Ti", "B"],
    "descriptor" :{
       "type":          "se_a",
       "sel":           [72, 72, 72, 72, 72, 92],
       "rcut_smth":      5.80,
       "rcut":          6.00,
       "neuron":         [25, 50, 100],
       "resnet_dt":      false,
       "axis_neuron":    16,
       "seed":          1,
       "_comment":       " that's all"
    },
    "fitting_net" : {
       "neuron":         [240, 240, 240],
       "resnet_dt":      true,
       "seed":          1,
       "_comment":       " that's all"
    },
    "_comment":     " that's all"
  },

  "learning_rate" :{
    "type":         "exp",
    "decay_steps":  5000,
    "start_lr":     0.001,
    "stop_lr":      3.51e-8,
    "_comment":     "that's all"
  },

  "loss" :{
    "start_pref_e": 0.02,
    "limit_pref_e": 1,
    "start_pref_f": 1000,
    "limit_pref_f": 1,
    "start_pref_v": 100,
    "limit_pref_v": 1,
    "_comment":     " that's all"
```

```
},

"_comment": " training controls",
"training" : {
    "systems":     ["../data/DeepData/ "],
    "set_prefix":  "set",
    "stop_batch":  3500000,
    "batch_size":  1,

    "seed":        1,

    "_comment": " display and restart",
    "_comment": " frequencies counted in batch",
    "disp_file":   "lcurve.out",
    "disp_freq":   100,
    "numb_test":   10,
    "save_freq":   1000,
    "save_ckpt":   "model.ckpt",
    "disp_training":true,
    "time_training":true,
    "profiling":   false,
    "Profiling_file":"timeline.json",
    "_comment":    "that's all"
},

"_comment":       "that's all"
```

Appendix B: Input File of Allegro

general

root: results/HEA_MB2_Mo

run_name: MB2_HEA_Mo_MODEL_HIRES_1

seed: 123456

dataset_seed: 123456

append: true

default_dtype: float32

-- network --

model_builders:

 - Allegro.model.Allegro

 # the typical model builders from `nequip` can still be used:

 - PerSpeciesRescale

 - ForceOutput

 - RescaleEnergyEtc

cutoffs

r_max: 6.0

avg_num_neighbors: auto

radial basis

BesselBasis_trainable: true

PolynomialCutoff_p: 6 # sets it BOTH for the RadialBasisProjection AND the Allegro_Module

symmetry

l_max: 2

parity: o3_full # allowed: o3_full, o3_restricted, so3

Allegro layers:

num_layers: 6

env_embed_multiplicity: 64

embed_initial_edge: true

two_body_latent_mlp_latent_dimensions: [64, 128, 256, 512]

two_body_latent_mlp_nonlinearity: silu

two_body_latent_mlp_initialization: uniform

latent_mlp_latent_dimensions: [512]

latent_mlp_nonlinearity: silu

latent_mlp_initialization: uniform

latent_resnet: true

env_embed_mlp_latent_dimensions: []

env_embed_mlp_nonlinearity: null

env_embed_mlp_initialization: uniform

- end allegro layers -

Final MLP to go from Allegro latent space to edge energies:

edge_eng_mlp_latent_dimensions: [128]

edge_eng_mlp_nonlinearity: null

edge_eng_mlp_initialization: uniform

-- data --

dataset: ase

dataset_file_name: HEA_MB2_Mo_MODEL_HIRES_1.extxyz   # path to data set file

ase_args:

  format: extxyz

A mapping of chemical species to type indexes is necessary if the dataset is provided with

atomic numbers instead of type indexes.

chemical_symbols:

  - Hf

  - Zr

  - Ta

  - Mo

  - Ti

  - B

```
# logging

wandb: True

wandb_project: MB2_HEA_Mo

verbose: info

log_batch_freq: 10


# training

n_train: 1000

n_val: 200

NEQUIP_NUM_TASKS: 64

batch_size: 15

max_epochs: 1000000

learning_rate: 0.001

train_val_split: random

shuffle: true

metrics_key: validation_loss


# use an exponential moving average of the weights

use_ema: true

ema_decay: 0.99

ema_use_num_updates: true
```

```yaml
# loss function

loss_coeffs:

  forces: 1.

  total_energy:

    - 1.

    - PerAtomMSELoss


# optimizer

optimizer_name: Adam

optimizer_params:

  amsgrad: false

  betas: !!python/tuple

  - 0.9

  - 0.999

  eps: 1.0e-08

  weight_decay: 0.


metrics_components:

  - - forces                    # key

    - mae                       # "rmse" or "mae"

  - - forces

    - rmse

  - - forces
```

```
    - mae

    - PerSpecies: True          # if true, per species contribution is counted separately

      report_per_component: False        # if true, statistics on each component (i.e., fx, fy, fz) will

be counted separately

    - forces

    - rmse

    - PerSpecies: True

      report_per_component: False

  - - total_energy

    - mae

  - - total_energy

    - mae

    - PerAtom: True


# lr scheduler, drop lr if there is no improvement for 50 epochs

lr_scheduler_name: ReduceLROnPlateau

lr_scheduler_patience: 50

lr_scheduler_factor: 0.5


# early stopping if max 7 days is reached or lr drops below 1e-5 or no improvement on val loss

for 100 epochs

early_stopping_upper_bounds:

  cumulative_wall: 604800.
```

early_stopping_lower_bounds:

  LR: 1.0e-5

early_stopping_patiences:

  validation_loss: 100